Journal of Energy Storage 45 (2022) 103751

Contents lists available at ScienceDirect

Journal of Energy Storage

journal homepage: www.elsevier.com/locate/est

Research Papers

Enriching the stability of solar/wind DC microgrids using battery and superconducting magnetic energy storage based fuzzy logic control

Kotb M. Kotb [a,c,*], Mahmoud F. Elmorshedy [a], Hossam S. Salama [b,c], András Dán [c]

[a] Electrical Power and Machines Engineering Department, Faculty of Engineering, Tanta University, Tanta 31521, Egypt
[b] Department of Electrical Engineering, Faculty of Engineering, Aswan University, Aswan 81542, Egypt
[c] Department of Electric Power Engineering, Faculty of Electrical Engineering and Informatics, Budapest University of Technology and Economics, Budapest 1111, Hungary

ARTICLE INFO

Keywords:
DC-bus microgrid
Battery storage system
Superconducting magnetic energy storage
Fuzzy logic control
Renewable energy

ABSTRACT

Utilizing robustly-controlled energy storage technologies performs a substantial role in improving the stability of standalone microgrids in terms of voltages and powers. The majority of investigations focused less on integrating energy storage systems (especially superconducting magnetic energy storage 'SMES') within DC-bus microgrids. Besides, implementing fuzzy logic control (FLC) for both batteries and SMES within the DC-bus microgrids to enrich their stability and power quality under extreme climatic and loading variations has been seldomly addressed. Consequently, this paper introduces a comparative analysis of the performance of a hybrid renewable PV/wind DC-bus microgrid that separately implements fuzzy-controlled battery and SMES systems to enhance the microgrid stability and power quality. The proposed FLC approaches supervise energy interchange inside the system, mitigate the DC-bus voltage fluctuations, and smooth out the load power during the different instabilities. The system is examined under distinct normal and extreme climatic fluctuations such as wind gusts and rapid shadow and under sudden balanced and unbalanced loading events. The proposed FLC approaches are established based on quantifying the DC-bus voltage variation and measuring the actual battery and SMES currents which can be employed directly for the control action; hence, reducing both calculations/calibrations and complexity of the control system. Besides, they offer very quick charging/discharging actions for both battery and SMES systems to mitigate unexpected and rapid variations efficiently. For the load side, the study proposes a variable modulation index control based-sinusoidal pulse width modulation for controlling the prime inverter to preserve the load voltage and frequency constant during both balanced and unbalanced loading and extreme climatic disturbances. The obtained findings confirmed the efficacy of the proposed approaches in enriching the microgrid stability. Besides, they unveiled the magnificent performance of SMES over batteries regarding the response time, peak over- and undershoot, load voltage profile, and load power smoothness.

1. Introduction

1.1. Background

Currently, renewable energies utilization is expanding globally for transmission and distribution systems to assist traditional energy production in supplying different loads. Governments worldwide are striving hard to expand the dependability of renewable energy sources (RESs) over the traditional energy sources owing to the different drawbacks concerned with last ones such as pollution, high cost, rapid depletion, and the burdensome regulations related to emissions of greenhouse [1]. Conversely, RESs have attractive merits over traditional ones since they are eco-friendly, require low maintenance, save money, and will not run out [2]. Therefore, both industry and research & development sectors have given much attention to reassure utilization of renewable energy sources (RESs) such as solar, wind, hydroelectric, and

Abbreviations: DC, Direct Current; AC, Alternating Current; SMES, Superconducting Magnetic Energy Storage; FLC, Fuzzy Logic Control; RESs, Renewable Energy Sources; PV, Photovoltaic; WT, Wind Turbine; ESTs, Energy Storage Technologies; MGs, Microgrids; MPPT, Maximum Power Point Tracking; TSR, Tip-Speed Ratio; INC, Incremental Conductance; SPWM, Sinusoidal Pulse Width Modulation; BSS, Battery Storage System; SOC, State of Charge.

* Corresponding author at: Department of Electric Power Engineering, Faculty of Electrical Engineering and Informatics, Budapest University of Technology and Economics, Budapest 1111, Hungary.
E-mail address: kotb.mohamed@f-eng.tanta.edu.eg (K.M. Kotb).

https://doi.org/10.1016/j.est.2021.103751
Received 27 September 2021; Received in revised form 1 December 2021; Accepted 3 December 2021
Available online 11 December 2021

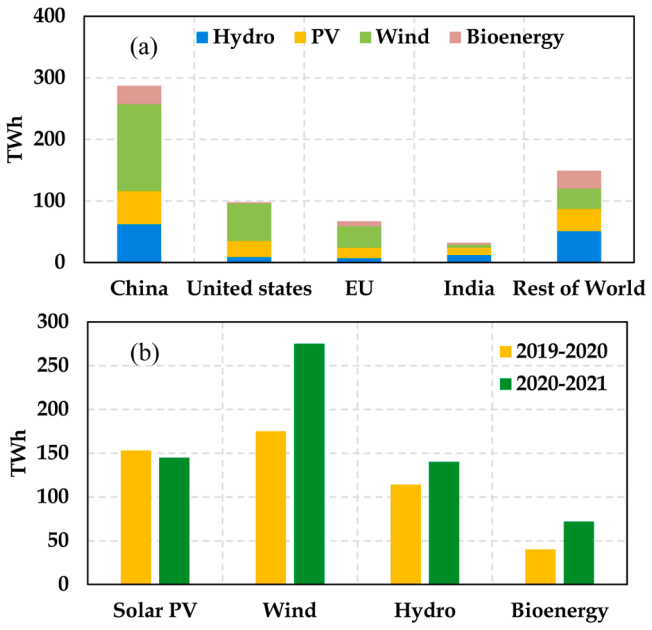

Fig. 1. Renewable energy production growth by (a) technology and country in 2020–2021, (b) technology in 2019–2020 and 2020–2021 [5].

wave [3]. Among the distinct RESs, photovoltaic (PV) and wind turbine (WT) systems are considered the most utilized, either individually or coupled, to supply a different kind of consumers in isolated or grid-connected systems due to their complementary time accessibility and the progressively decreased acquisition costs [4]. This significant expansion and dependability on RESs, especially solar PV and wind energies, can be realized from the latest statistics provided by the International Energy Agency (IEA) shown in Fig. 1 [5]. According to the IEA, energy production from RESs in 2021 is placed to reach 8300 TWh (> 8% growth), the expansion which is considered the quickest since 1970. Besides, From Fig. 1 a, electricity production from both solar PV and wind provide about 68% of RESs growth with China only interpret for about 50% of the worldwide growth in RESs electricity in 2021, afterward the United States, the European Union, India, and then the rest countries. From Fig. 1 b, generation from wind energy has the leading growth in renewable generation by 275 TWh which is considerably more than 2020 levels. Since China remains the major PV market in the world, substantial decrease in new solar PV capacity additions in 2020 due to Covid-related delays; even though 2021 is not over yet, the generation levels from solar PV are equivalent to the 2020 levels [5]. Although this year-on-year expansion in RESs utilization, the major challenge of the PV and WT systems remains the climatic dependency in which the produced power depends on meteorological conditions like temperature, solar radiation, and wind speed. Hence, the electrical power system steadiness will be influenced by these fluctuations [6].

To overcome the intermittency problem, energy storage technologies (ESTs) are integrated with RESs to benefit from the generated energy and keep it for later use; thus, reducing the lack of other sources. The significant influence of utilizing ESTs in power grids, particularly the standalone microgrids (MGs), alleviates the energy exchange from/to the grid during regular and irregular circumstances; thus, ESTs can play a significant role in enhancing the stability of these MGs [7]. These storage elements act as a fast-pulsating power supply capable of enhancing the energy interchange among energy system components, preserving system security and self-resiliency during eventuality disturbances [4]. Thus, the integration between ESTs and RESs becomes essential to lessening the sporadic accessibility of renewable resources. Based on a comprehensive and statistical analysis assessment of PV-WT hybrid renewable system considering more than 550 relevant articles since 1995 [8], battery storage system (BSS) was employed in 77% of the studies, followed by hydrogen tanks (15.4%). In contrast, other ESTs such as hydraulic storage, superconducting magnetic energy storage (SMES), supercapacitors, flywheel, and compressed air accounted for 7.6% of the studies. Power capabilities and the run-time are considered the key issues in manufacturing ESTs; hence, two kinds of ESTs are classified; the first includes high power density, and the second includes high energy density [9]. The high spread of utilizing BSSs is due to their response time, scalability and modularity, the ability to supply various ancillary services, and the ability to be integrated with other ESTs [10]. Besides, BSSs are distinguished by a high energy density; hence, they are appropriate for use with small and regular load variants. However, the main cons of BSSs include the availability of a restricted number of full discharge cycles, environmentally unfriendly, and their thermal fugitive that can arise with incorrect charging [11,12]. Meanwhile, the SMES is considered one of the incredibly substantial ESTs in the application of PV-wind hybrid energy systems. The different instabilities can be alleviated by utilizing SMES for fast charging/discharging energy from/to the MG. The SMES is characterized by the rapid response due to its high power density, long lifetime and high efficacy compared to other ESTs; conversely, the main challenges that hinder its comprehensive implementation is the bulky size and the high cost [12,13]. The different ESTs, including BSSs and SMES, can be integrated into the different structures of MGs (i.e., AC MGs, DC-bus MGs, and hybrid AC-DC MGs). The major disparities among the different MG structures can be found [14] and [15]. Besides, the interface system between the ESTs and MG and the control complexity depends on their construction, their configuration (distributed, aggregated or hybrid), and the MG structure [11,16]. Different control approaches have been proposed in different studies to control the behavior of ESTs and the entire MG robustly. By addressing different relative studies, the proportional-integral (PI) controller, hysteresis control, and fuzzy logic control (FLC) are the most used tools for building up EST control strategies integrated with renewable MGs. In this study, a comparative assessment is conducted between the performance of fuzzy-controlled battery storage and SMES systems integrated separately into a PV/WT DC-bus MG. In this regard, several studies that addressed the behavior of BSS or SMES with MGs have been investigated and analyzed in the following subsection.

1.2. Literature survey

In [17], authors integrated a PI-controlled SMES unit with a standalone hybrid wind generating system comprising doubly fed induction generator (DFIG) and permanent magnet synchronous generator (PMSG) to minimize the output power fluctuations and enhance the system power quality. However, the impact of load variations was not investigated, and only normal wind speed variations were addressed. Another study investigated the voltage and frequency stability enhancement using a fuzzy-controlled SMES unit integrated with squirrel cage induction generator (SCIG) & DFIG wind system and connected to the grid was presented in [18]. However, the study addressed only the impact of load insertion/rejection on the system performance without considering wind activity or load changing. Meanwhile in [19], the SMES was used to overcome the fluctuations caused by the high penetration level of PV generators in a grid-connected AC MG where a PI control and FLC schemes were developed to enhance the system reliability. The control schemes were examined for solar radiation and loading variations and also for sudden grid disconnection. Further, the energy management of a standalone WT/BSS/SMES DC-bus MG controlled with a PI-controller was examined in [20]. The system was examined under different unsteady meteorological and loading conditions and also for pulse loading occasions. Authors in [21] applied both PI and FLC schemes for a standalone PV/diesel AC MG to improve the stability and energy exchange within the MG. The system stability was assessed under the insertion/rejection of PV units and loads. The change in frequency and SMES current were

Table 1
Comparison among the most featured studies in the literature with the current study.

Ref.	Utilized RESs		MG type	Grid-		Utilized ESTs		EST controller		MPPT		Load (v, f) control	Addressed events		
	PV	WT		on	off	BSS	SMES	PI	FLC	PV	WT		Climatic activity		Load variation
													Normal	Extreme	
[17]	x	√	AC	x	√	x	√	√	x	x	x	x	√	x	x
[18]	x	√	AC	√	x	x	√	x	√	x	x	NA	x	x	x
[19]	√	x	AC	√	x	x	√	x	√	√	x	NA	x	x	x
[20]	x	√	DC	x	√	√	√	√	x	x	√	x	√	x	x
[21]	√	x	AC	x	√	x	√	x	√	√	x	x	x	x	x
[22]	√	x	DC	x	√	√	x	x	√	x	x	x	√	x	√
[23]	√	x	DC	x	√	√	x	x	√	x	x	x	√	x	√
[24]	√	x	AC	√	x	√	√	√	√	x	x	NA	x	x	√
[25]	√	√	DC	√	x	√	x	x	√	√	√	NA	x	x	x
[26]	√	x	AC	√	√	√	x	x	√	x	x	NA	x	x	x
[27]	√	√	AC	√	x	x	√	x	√	√	x	NA	x	√	√
Current study	√	√	DC	x	√	√	√	x	√	√	√	√	√	√	√

utilized as fuzzy inputs while the interfacing voltage source converter was controlled using the PI controller. However, the extreme variation in wind speed (wind gusts) were not addressed. In [22], a FLC scheme was suggested to regulate the bus voltage and adjust the power stability of a DC-bud MG incorporating PV/BSS and a fuel cell. The control system was validated under different dynamic instabilities in load demand, solar radiation, and overloading situations. Nevertheless, no maximum power point tracking (MPPT) was employed for the PV system, and the load voltage/frequency control was not clarified enough.

Another FLC scheme was suggested in [23] to coordinate the power flow between PV generator and BSS in a DC-bus MG. The suggested controller enhanced the usage of both PV and BSS powers and kept the battery state of charge (SOC) within their boundaries despite climatic or load demand variations. However, the authors suggested a load shedding possibility to avoid SOC from reaching its minimum value and a PV power curtailment for overcharging protection. Nevertheless, the load side control, including load voltage and frequency stabilization, was not addressed. Authors in [24] utilized a SMES unit based on a shunt active power filter for alleviating power fluctuations, restricting harmonic currents in a grid-connected AC MG including a PV system and supplying different kinds of loads (balanced, unbalanced, nonlinear, and pulsating load). Nevertheless, the influence on including WTs in the system and the extreme loading and renewables' variations were not addressed. An intelligent energy management based on combined FLC and fractional-order PID controller for a PV/WT/BSS DC-bus MG was presented in [25]. However, the DC-link and load voltages and the load power still contained oscillations around the reference value. Also, the effectiveness of the proposed scheme was not attested during wind gusts and loading events. A coordinated BSS control based on FLC for a PV grid-on/off AC MG with modified AC coupling configuration was examined in [26]. Both the PV system and grid side converter were regulated using conventional PI controllers. However, the presented load demand power was found to contain spikes and over/undershoots. Besides, this study did not address the influence of the extreme variations in solar radiation and load demand to verify the effectiveness of the proposed control scheme. In [27], the authors proposed a fuzzy-controlled SMES integrated with a grid-connected PV/WT AC MG to mitigate the instabilities of active/reactive powers exchange. The system was examined under wind gusts and load variations in which the line power loss was also investigated. However, authors accomplished the work by considering only the grid-connected mode and also by comparing the system performance once with SMES and once without while comparison with other ESTs is found better be addressed. For better clarifying the disparities among the different addressed studies, Table 1 summarizes a comparison among the investigated studies and the presented work.

For providing a broad overview of authors concerns in this field, data for keywords with at least ten occurrences were collected from the Scopus database, and individual clusters, which included both a network visualization (Fig. 2 a) and overlay visualization (Fig. 2 c) were merged. These clusters are suggestive of publications with relative use of keywords in their publications. Among a total of 2879 observed keywords, 39 meet up the level of 10 occurrences. Fig. 2 (a, b) display that the keyword "dc microgrid" is interrelated with battery energy storage, power quality, energy management, voltage control, renewable energy sources, pi controller, and fuzzy logic control, signifying how the DC-bus MGs is considered an attractive solution as a robust power system with high power quality. Besides, Fig. 2 (a, d) demonstrate that the keyword "superconducting magnetic energy storage" is unified with the words microgrid, wind turbine and photovoltaic, fuzzy logic control, energy management, electric vehicles, and battery storage system, which notified that there is very few or no correlations between the integration of SMES with DC-bus MGs. This intense exploration was validated by the dense connections and proximity between the keywords. Also, the occurrences average year is emphasized by the colours legend in the overlay visualization shown in Fig. 2 d.

1.3. Research gaps and study contributions

Based on the literature review and Table 1, which are presented in the previous subsection, most of the case-studies investigated the integration of single RES with ESTs within the AC microgrid structure. Moreover, applying SMES systems with hybrid PV/wind systems, DC-bus MGs got less attention from researchers. Besides, the adoption of FLC for both battery and SMES systems in DC-bus MG has not been implemented widely like the implementation of MPPT techniques for either PV or wind systems. Furthermore, the formerly-presented control techniques, especially those based on FLC for DC-bus MGs, utilized both voltage deviation and change in voltage deviation as fuzzy inputs, requiring additional calculations and calibrations. Moreover, these studies have not considered the fast charging/discharging in their fuzzy rules, which can significantly improve controller performance. To add, the unbalanced load events have been investigated in only a few number of previous studies which dealt with the hybrid PV/WT microgrids. Also, the high and fast variations of wind speed and solar radiation have not been investigated in most similar studies. Therefore, this study aims to satisfy the existing research gaps by comparing a hybrid renewable PV/wind DC-bus MG that integrates the fuzzy-controlled battery and SMES systems separately. In short, the main contributions of the current study can be digested as follows:

- Developing a comparative assessment between the impact of separately integrating a fuzzy-controlled battery and SMES systems into a hybrid renewable PV/wind DC-bus MG considering extreme variations of meteorological conditions such as wind gusts and rapid shadow, and sudden load changes including balanced/unbalanced

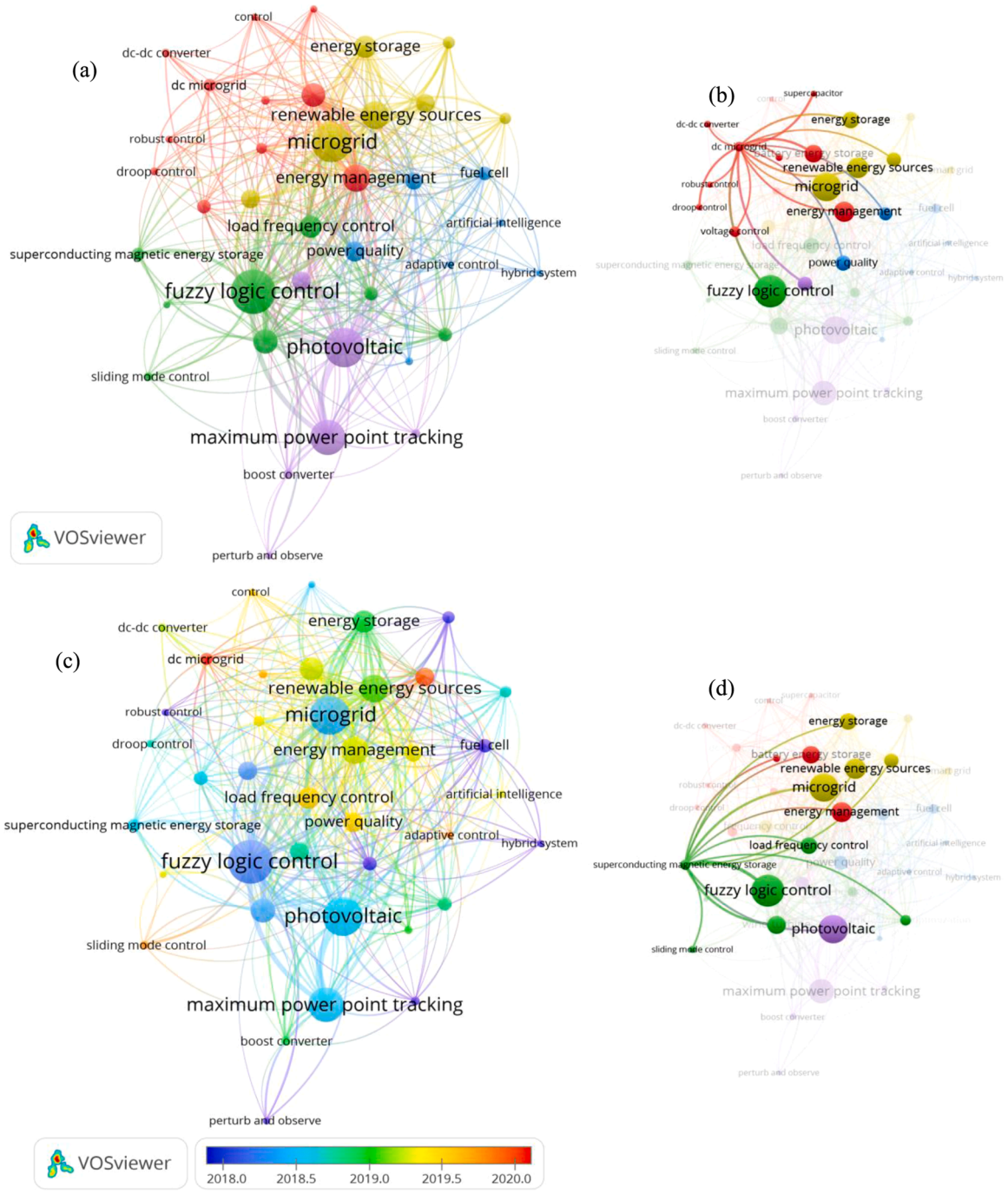

Fig. 2. Author keywords co-occurrences in publications related to PV/WT and controlled BSS/SMES research between 2010 and 2021 (a, b, d) network visualization, (c) overlay visualization.

loading events which have been seldomly investigated in relative literature.

- The proposed FLC is established based on measuring the DC-bus voltage change and the actual current of both battery and SMES systems; these currents are employed directly for the control action, reducing both calculations/calibrations and complexity of the control system.
- Alleviating the different deviations of DC-bus voltage and smoothing out both DC-bus power and load demand power produced by the distinct fluctuations using the proposed FLC schemes. The proposed FLC schemes offer quick charging and discharging actions of both battery and SMES systems to effectively mitigate the occurring meteorological and load variations.
- Preserving the load voltage and frequency constant by means of the proposed prime inverter control approach during both balanced and unbalanced loading and extreme climatic disturbances utilizing the variable modulation index control strategy.

1.4. Organization of the manuscript

Besides the introduction presented in this section, this study's materials and proposed methods are offered in Section 2, which involve the detailed modeling of the system's components and the developed control approaches. The most crucial outcomes are provided and analyzed in Section 3, including detailed comparisons between the two energy storage technologies, while the main conclusions and outlook

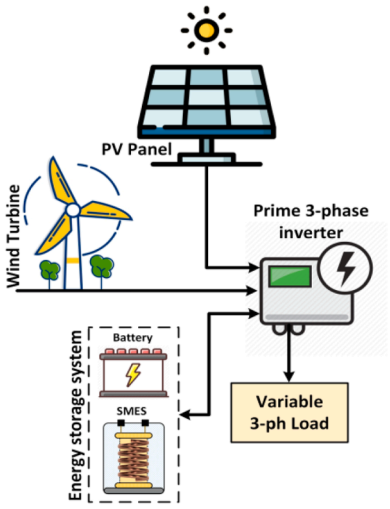

Fig. 3. Schematic diagram of the examined system.

Table 2
Practical specifications of the employed PV system.

Parameter	Value	Parameter	Value
Nominal capacity/module	305 W	Efficiency at STC	13%
Rated operating temperature	25 °C	Open circuit voltage	321 V
Derating factor	85%	Short circuit current	18.4 A
Temperature coefficient	−0.386%/°C	V_{MPP}, I_{MPP}	273.5 V-22.32 A
Parallel strings	4	Series strings	5

suggestions are given in Section 4.

2. Materials and methods

This section is divided into two subsections; the system description is first introduced to provide the detailed modeling and specifications of the system's elements, including the PV units, the wind-driven generator, the EST including batteries and the SMES and the prime inverter. The second subsection affords the implementation of the proposed control methods, including the generation-side control, the energy storage control, and the load side management.

2.1. System modeling and description

Fig. 3 illustrates a schematic diagram of the studied system, consisting of a generation side represented in the PV panels and the WTs, an energy storage system (batteries or SMES), and a variable three-phase load fed from the prime inverter. The generated energy through the hybrid system can be supplied immediately to the load, and when the generated energy surpasses the load demand, the extra energy is distributed to the EST. As exhibited in Fig. 3, the load is connected directly to the AC side, whereas the PV panel, the WT, and the EST are connected to the DC side. The supply precedence is that the generated energy fulfills the load demand while the EST contributes once the generated energy is insufficient. If the energy demand becomes greater than the generated energy, then, in this case, the insufficient generated energy is considered a loss of power supply. Conversely, when both the PV panels and the WTs productively satisfy the load demand and the EST is too full to accept more power, the surplus power can then be distributed to supply a dump load that can be utilized for heating rationale. The mathematical modeling illustration of the system's elements is provided in the upcoming paragraphs with the necessary equations.

Table 3
Technical specifications of the employed wind turbine and the PMSG.

The wind turbine		The PMSG	
Parameters	Value	Parameters	Value
Rated capacity	7.5 kW	Rated power	6 kW
Cut-in wind speed	4 m/s	Rated current	12 A
Cut-out wind speed	12 m/s	Rated speed	153 rad/sec
Rotor diameter	3.2 m	Rated torque	40 N.m
Inertia	7.5 kg.m^2	Stator inductance	8.4 mH
Friction coefficient	0.06 N.m.s/rad	Armature resistance	0.4 Ω

2.1.1. The solar PV system

The PV panels are considered one of the key components in the examined system, which convert solar energy into electricity. SunPower SPR-305-WHT solar PV panels with 13% efficiency and rated output power of 305 W are employed to obtain a PV system capacity of 6.25 kW. The PV modules' efficiency and output power function the solar radiation and the operating temperature as demonstrated by Eqs. (1)–(3) [28]. The practical data of the utilized PV panels are listed in Table 2.

$$P_{pv} = P_{pvR} D_{pv} \left(\frac{\lambda}{\lambda_{STC}}\right) \times \left[1 + \sigma\left(T_{pv} - T_{pv,STC}\right)\right] \tag{1}$$

$$\eta_{pv} = \eta_{pv,STC}\left[\alpha log_{10}(\lambda) + \left(1 - \sigma\left(T_{pv} - T_{pv,STC}\right)\right)\right] \tag{2}$$

$$T_{pv} = T_a + \lambda\left[\frac{T_n - 20}{\lambda_{STC}}\right] \tag{3}$$

where P_{pvR} is the rated power of the PV panels (kW), D_{pv} is the derating factor (%), λ is the average hourly solar radiation falling on the PV panel at operating temperature (kW/m^2), λ_{STC} is the solar radiation at standard test conditions "STC" (1-kW/m^2), σ is the temperature coefficient, T_{pv} is the PV cell temperature, $T_{pv,STC}$ is the PV cell temperature at STC, $\eta_{pv,STC}$ is the PV cell efficiency at STC, α is the intensity coefficient, T_a is the ambient temperature, and T_n is the nominal operating cell temperature.

2.1.2. The wind energy system

The employed wind energy system mainly incorporates a vertical-axis turbine coupled with a PMSG. Table 3 lists the technical specifications of the utilized wind turbine and the PMSG. For a typical WT, the output power varies based on several parameters in which the wind energy is transformed to electrical energy, as indicated in Eq. (4) [29]. The output power can be conveyed in terms of the wind speed as in Eq. (5) [30]. Moreover, the wind power coefficient (C_p) can be determined by Eqs. (6)–(7) where the coefficients C1-C6 are taken from [31,32].

$$P_{WT} = 0.5\rho A V^3 C_p(\lambda, \beta) \tag{4}$$

$$P_{WT} = \begin{cases} P_{WT}\left(\dfrac{V - V_{cin}}{V_n - V_{cin}}\right) & if\ V_{cin} < V < V_n \\ P_{WT} & if\ V_n \le V < V_{coff} \end{cases} \tag{5}$$

$$C_p = C_1\left(\frac{C_2}{\lambda_i} - C_3\beta - C_4\right)e^{\frac{C_5}{\lambda_i}} + C_6\lambda \tag{6}$$

$$\frac{1}{\lambda_i} = \frac{1}{\lambda + 0.08\beta} - \frac{0.035}{\beta^3 + 1}, \lambda = \frac{R\omega_r}{V} \tag{7}$$

2.1.3. The battery energy storage system

ESTs are usually regulated to oversee the energy trade amongst the generation and load sides during normal and abnormal conditions. Moreover, the responsibility of ESTs become essential, particularly when maximum exploitation of renewable energies is applied. A battery

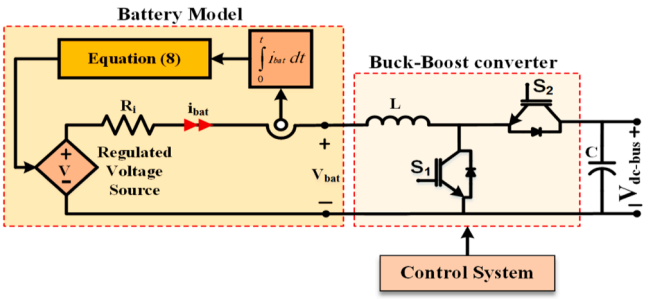

Fig. 4. Typical equivalent circuit of a battery controlled with a buck-boost converter.

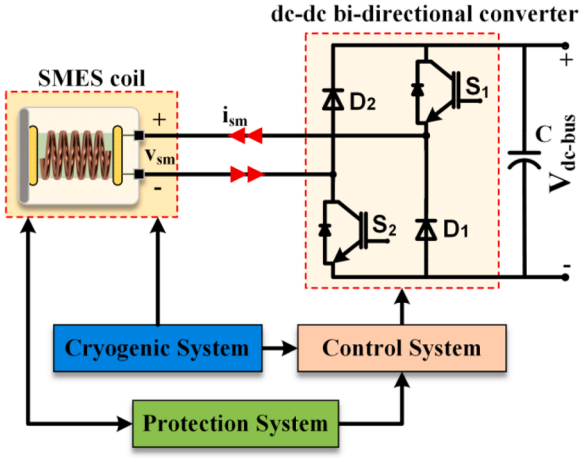

Fig. 5. Typical construction of a SMES system connected to a DC-bus MG.

standard model is used in the current study in which the battery state of charge (SOC) is considered a state variable to prevent the arithmetic loop complexity and facilitate indicating four types of batteries, including the lead-acid type utilized in the study [33]. The model represents the battery by a regulated voltage source and a fixed resistance as described in Fig. 4 and emphasized by Eqs. (8), (9) [33].

$$V = V_0 - \frac{V_{Pol}C_{bat}}{C_{bat} - \int_0^t i_{bat}dt} + A\exp\left(-B\int_0^t i_{bat}dt\right) \tag{8}$$

$$V_{bat} = E - R_i.I_{bat} \tag{9}$$

From the previous relations, V, V_0, V_{Pol}, C_{bat}, $\int i_{bat}\,dt$, A, and B are the no-load voltage, the battery constant voltage, the polarization voltage, the battery capacity, the actual battery charge, the exponential zone amplitude, and the exponential zone time constant inverse, respectively. On the other side, V_{bat} refers to the battery voltage, R_i to the internal resistance, and i_{bat} to the actual battery current. The lead-acid batteries are typified by the potential of offering large current for a short period; therefore, they are the best trendy alternative in hybrid energy systems [34]. The battery capacity must sustain the load requirement for more prolonged intervals in the possibility of decreased solar or wind accessibility. The battery capacity can be evaluated using Eq. (10), in which a 50 Ahr battery is incorporated in the system and capable of delivering 6 kW to the load demand in one hour. The battery terminal voltage (V_{bat}) and its depth of discharge (DoD) are considered as 300 V and DoD = 0.6, respectively [35].

$$C_{bat} = \frac{E_{demand}}{V_{bat} * DoD} \tag{10}$$

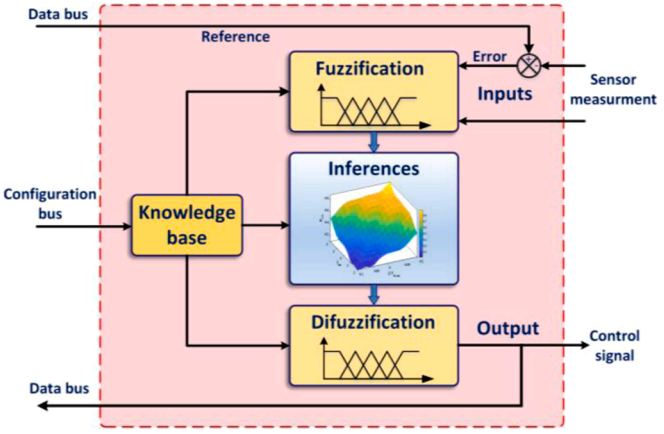

Fig. 6. Procedure of the fuzzy logic control.

2.1.4. The SMES system

Essentially, energy storage technologies convert the energy from the electrical form to another form based on the utilized technology. For the SMES system, the electrical energy is stored in a magnetic form generated by a circulating current through a superconducting coil [36]. Fig. 5 shows the core components of a typical SMES system which consists of a superconducting coil, cryogenic system, protection system, and control system. When the SMES is integrated with AC MGs, a power conversion/conditioning system serves as an interface stage between the SMES and the MG [37]. The current study connects the SMES system directly to the DC-bus MG through the bi-directional dc-dc converter. The superconducting coil is considered the heart of the SMES system since it is responsible for storing the energy. This coil is made of superconducting materials, such as Mercury or Niobium–Titanium, which is kept cold enough by the cryogenic refrigerator system to sustain the superconducting state in the wires; hence, the coil can provide zero resistance and zero losses [38]. The protection system protects the SMES unit from irregular actions while the control system connects power demands from/to the grid with power flows to/from the SMES coil [39]. The SMES has several advantages in comparison with other ESTs as follows [40]:

- The direct storage of electrical energy permits response times in milliseconds.
- The SMES has no moving elements, and currents in the SMES coil experience nearly zero resistance, the matters which increase its efficacy.
- The SMES has a high level of efficiency, which can reach up to 98%.
- The quantity of charges/discharges have almost no impact on the SMES lifespan.

From the economic viewpoint, based on the financial data provided in [40], the SMES has a moderate cost compared with other ESTs; also, the SMES lies in a suitable place among different ESTs based on the price of its specific power density. Likewise, the operating and maintenance costs of SMES are reasonably comparable with various ESTs.

The stored energy, measured in Joules, as a function of coil inductance (L_s) and SMES current (I_s), is described in Eq. (11), while the SMES power in Watts, as a function of SMES voltage (V_s), is given in Eq. (12) [21]. In this study, a SMES coil of 1.5 H of 300 A initial current is employed in the 67.5 kJ SMES unit and connected to the DC-bus via an 8.6 mF capacitor.

$$E_{sm} = 0.5I_{sm}^2 L_{sm} \tag{11}$$

$$P_{sm} = \frac{dE_{sm}}{dt} = L_{sm}I_{sm}\frac{dI_{sm}}{dt} = V_{sm}I_{sm} \tag{12}$$

$$\mu_A(x) = \begin{cases} 0, & x \le a \\ \dfrac{x-a}{m-b}, & a < x \le m \\ \dfrac{b-x}{b-m}, & m < x \le b \\ 0, & x \ge b \end{cases}$$

$$\mu_A(x) = \begin{cases} 0, & (x < a) \text{ or } (x > d) \\ \dfrac{x-a}{b-a}, & a \le x \le b \\ 1, & b \le x \le c \\ \dfrac{d-x}{d-c}, & c \le x \le d \end{cases}$$

$$\mu_A(x) = e^{-\frac{(x-m)^2}{2k^2}}$$

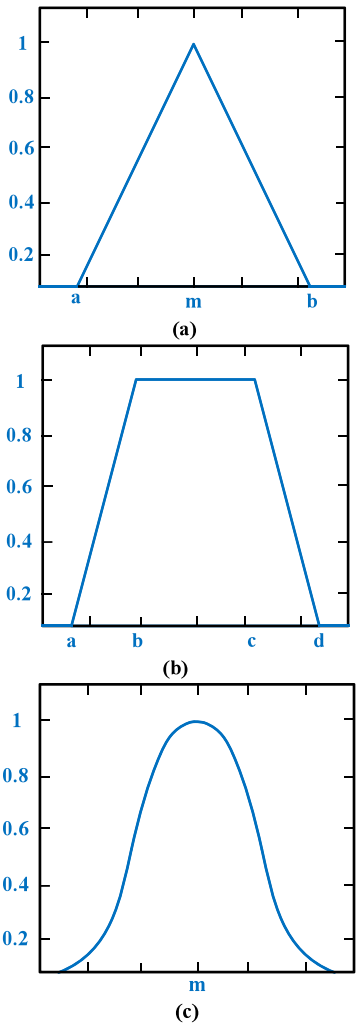

Fig. 7. Different membership functions of FLC (a) Triangular (b) Trapezoidal (c) Gaussian.

2.1.5. The fuzzy logic control

The fuzzy logic controllers are favored over the traditional controllers since they are more vigorous and can include a significantly broader range of operating conditions than the PI controllers [6]. Besides, FLC can run through noise and disturbances of distinct kinds. Also, utilizing a FLC is considerably inexpensive than acquiring a model-based controller for the same application. Moreover, FLCs are simpler to recognize and adjust their rules, are customizable, and use natural linguistic expressions [41]. The FLC is accomplished using the procedure shown in Fig. 6. The Fuzzification stage contains the functions that have two main tasks: read, measure, and scale the control variables and, secondly, convert the numerical values to the subsequent linguistic variables, which are fuzzy variables with suitable membership values. The knowledge base module includes the fuzzy membership functions described for every control variable and the essential rules that stipulate the control objectives by linguistic variables. The inferences module must be capable of imitating human decision-making and manipulating the control behaviors based on fuzzy logic. The Defuzzification module converts the implied decision from the linguistic variables into the numerical values.

The FLC is executed with the graphical user interface running with MATLAB environment. In this study, different membership functions such as triangular-type, trapezoidal-type, and Gaussian-type are utilized to fuzzify both inputs and output with different numbers of sets for the membership degree. The triangular function is described by a lower limit a, an upper limit b, and a value m, where a < m < b as described in Fig. 7 a. The trapezoidal function is specified by a lower limit a, an upper limit d, a lower support limit b, and an upper support limit c, where $a < b < c <$ d as in Fig. 7 b. The Gaussian function is defined with a central

Table 4
Comparison among the FLC and other control techniques.

Item/Controller	PID	FLC	MPC
Flexibility	Low	High	High
Simplicity	Easy	Easy	Complex
Tuning	Hard	Relatively Hard	Complex
Out the control possibility	Yes	No	No
Control modification	Easy	Easy	Complex
Efficiency	Moderate	High	High
Handling systems	Linear+nonlinear	Linear+nonlinear	Linear+nonlinear
Disturbance minimization	Moderate	High	High
Adaptation	Yes	Yes	Yes
Number of inputs/ outputs	SISO	MIMO	MIMO
System forecasting	No	Yes with AI	Yes
Switching frequency	Fixed	Fixed	Variable

Abbreviations: ***PID****: Proportional-Integral-Derivative;* ***FLC****: Fuzzy Logic Control;* ***MPC****: Model Predictive Control;* ***SISO****: Single Input Single Output;* ***MIMO****: Multiple Inputs Multiple Outputs;* ***AI****: Artificial Intelligence.*

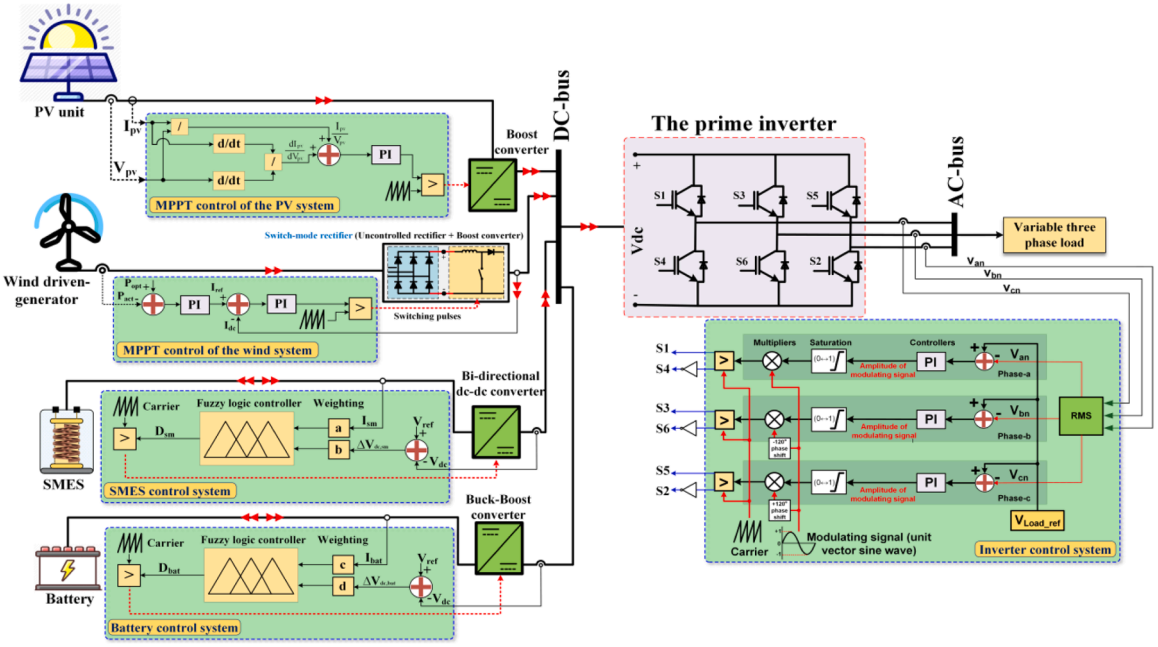

Fig. 8. Overall block diagram of the employed controllers in the system.

Table 5
Functionality and different disparities among the employed control configurations.

Control configuration	Objectives	Control method	Used controller
PV system control	• Extract the maximum power from solar energy • Match the generated voltage with the DC-bus voltage	Incremental Conductance	PI
WT control	• Extract the maximum power from wind energy • Match the generated voltage with the DC-bus voltage	Tip Speed Ratio	PI
Battery controller	• Synchronize the energy exchange between	Proposed	FLC
SMES controller	generation and load sides • Preserving the DC bus voltage constant • Smoothing out the load power as a result of maintaining the DC bus voltage constant	Proposed	FLC
Prime inverter controller	• Regulate the load voltage and frequency • Overcoming suddenly balanced and unbalanced load variations	Proposed variable modulation index-based SPWM	PI

value m and a standard deviation $k > 0$, as shown in Fig. 7 c.

In order to highlight the different features of FLC, Table 4 summarizes a comparison to show the distinct disparities among the FLC and other control techniques.

2.2. Methods

In order to investigate and assess the reliability performance of the DC-bus MG in the presence of two different energy storage elements, a comparative approach is selected to exhibit the distinct disparities of integrating batteries and SMES individually into the MG. Since the examined system principally depends on the generation from renewable resources, characterized by unpredictable nature, the produced power can be greater or fewer than the load requirement. Hence, robust controllers are principally mandatory to improve the whole system's functioning during regular and irregular circumstances. Fig. 8 demonstrates a detailed system structure besides the implemented control approach for each system element. In this figure, particular MPPT controllers are implemented to extract the maximum possible power from both solar and wind systems. Besides, FLC is applied to supervise the operation of batteries and SMES systems by providing the optimal duty cycle. For the load side, a variable modulation index control approach is employed to the prime inverter to sustain the load voltage/frequency constant all the time. Table 5 summarizes the functionality and disparities among the utilized control configurations in the presented study. For clear demonstration, a detailed explanation of each control approach is presented in the following subsections.

2.2.1. MPPT of the PV system

The performance of the PV units changes with the change of solar radiation and weather temperature according to the PV characteristics. At high weather temperatures, PV units' output power and efficiency are reduced while the elevated solar radiation boosts both output power and efficiency. Therefore, to obtain the maximum possible power from solar energy, it is essential to preserve the PV output voltage at the maximum power point (V_{mpp}), which can be accomplished using MPPT techniques. A maximum power point tracking based on the incremental conductance (INC) technique is employed in this study to extract the maximum possible power from solar energy. The INC technique has significant performance for tracking the PV peak output and enhancing the dynamic performance during rapidly fluctuating circumstances due to its blind compatibility with any PV type, the facileness of implementation on digital controllers, and its low cost and high- performance integrability with industrial inverters [42]. The setpoint of the boost converter's duty cycle is moderated automatically to obtain the desired voltage and current where the maximum power occurs at. The voltage and current at the PV array terminals are first measured as indicated in the flowchart describing the procedure of the INC method in Fig. 9. The INC technique produces the boost converter current reference value that relies on the signs of the variation in the power and voltage compared to the previous step. At each step, the incremental value is used to define

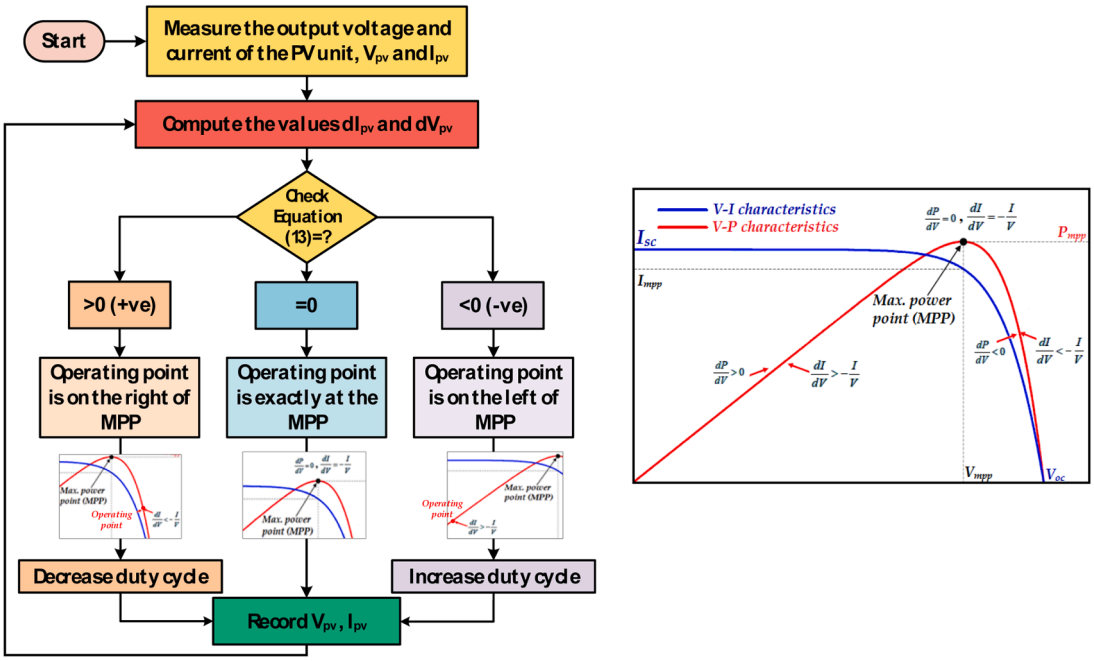

Fig. 9. MPPT control procedure of the PV system-based INC method.

the new value of the converter's current reference, where it was chosen as a trade-off between the power oscillation and the MPPT speed. Eqs. (13) and (14) show the INC technique main idea depending on the P-V curve [43]. As per Eq. (13), there are three prospects:

- If Eq-13=zero, the operating point is exactly at the top of the P-V curve (at the maximum power point 'MPP'), and the measured voltage and current are equal to the voltage at maximum power point (V_{MPP}) and the current at maximum power point (I_{MPP}), respectively.
- If Eq-13≠zero, this means that the PV voltage is greater or fewer than (V_{MPP}); hence, the sign of Eq-13 determines the direction of the next perturbation to drive the operating point towards the MPP. In this case, there are two different prospects:
  - a If the sign of Eq-13 is positive, the PV voltage is greater than V_{MPP}, and the operating point is located on the right of the MPP. Therefore, the MPPT controller reduces the duty cycle to force the operating point to move in the MPP direction.
  - b If the sign of Eq-13 is negative, the PV voltage is less than V_{MPP}, and the operating point is located on the left of the MPP. Hence, the MPPT controller raises the duty cycle to push the operating point to move in the MPP direction.

The previous steps are repeated until fulfilling (13), which successively grants the tracking system remains to run at the last operating point, awaiting any discovered variation.

$$\frac{dP_{PV}}{dV_{PV}} = 0 \rightarrow \frac{d(V_{PV}I_{PV})}{dV_{PV}} = 0 \rightarrow I_{PV} + V_{PV}\frac{dI_{PV}}{dV_{PV}} = 0 \tag{13}$$

$$\frac{dI_{PV}}{dV_{PV}} = -\frac{I_{PV}}{V_{PV}} \tag{14}$$

2.2.2. MPPT of the wind system

The PMSG employed in the wind system in this study is connected to the DC-bus or the DC grid via a switch-mode rectifier which consists of a three-phase uncontrolled rectifier (diode-based structure) followed by a controlled DC-DC boost converter as illustrated in Fig. 8. The generated AC electricity is converted and regulated to DC throughout two main stages; the first stage converts the generated variable AC electricity into DC, then regulated to a fixed DC voltage using a controlled DC-DC boost converter. As a result, the generated voltage can match the fixed/desired value of the DC-bus voltage during the different variations in the generation side.

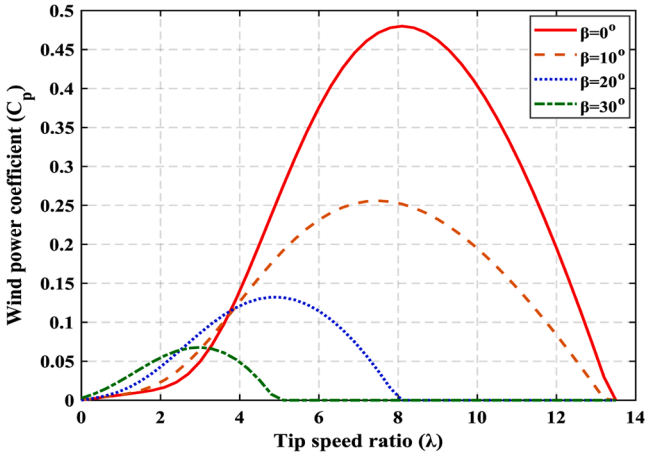

Fig. 10. The C_p-λ behavior at different values of pitch angle (β).

Different MPPT techniques can be employed to control the operation of the boost converter by regulating its duty cycle to achieve the desired control objectives. The most extensively recognized MPPT techniques which are developed for variable speed wind turbines are the perturb and observe (P&O) method, the wind speed measurement (WSM) or the tip-speed ratio (TSR) method, and the power signal feedback (PSF) method [43]. The WSM method necessitates the determination of the TSR, which is the ratio of the turbine blade speed to the wind speed and both wind speed and turbine speed as feedback signals [44]. The wind power coefficient (C_p) is calculated using Eqs. (6) and (7) which previously described in subsection (2.1.2), in which it can be remarked that it mainly depends on two variables, the TSR (λ), which can be found in Eq. (7) and the blade pitch angle (β). Therefore, the relationship between λ and C_p differs based upon the blade pitch angle value; this can be easily observed from Fig. 10, in which it can be recognized that the power coefficient can be maximum (C_{pmax}) at only one value of TSR, the

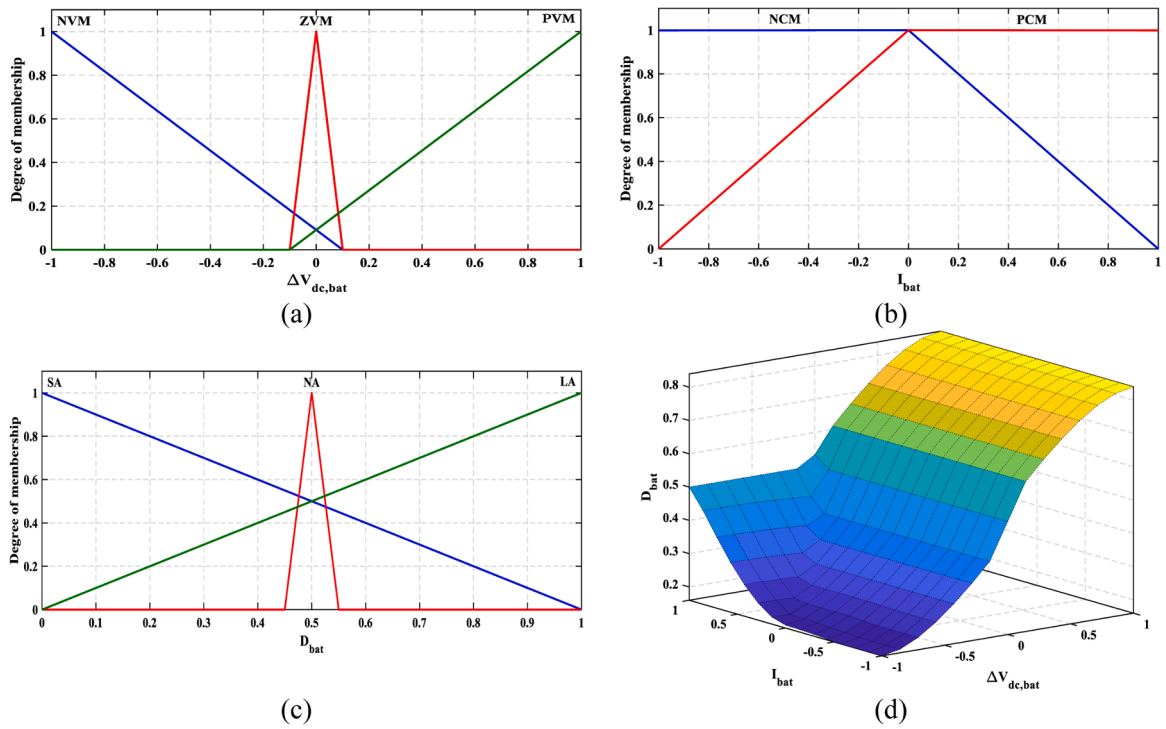

Fig. 11. Membership functions used for battery control (a) Input-1, $\Delta V_{dc,bat}$ (p.u), (b) Input-2, I_{bat} (p.u), (c) The output D_{bat}, and (d) 3-D graph of inputs-output membership functions.

optimal TSR (λ_{opt}).

It should be noted from Eq. (7) that the rotor speed should change when the wind speed is changing to sustain λ at its optimal value. Consequently, if β equals zero (means no pitch angle control), the maximum power coefficient, C_{pmax}, can be obtained, hence by substituting in Eq. (5), the optimal wind power (P_{opt}) can be determined. The MPPT technique employed for the wind system, shown in Fig. 8, consists of two cascaded PI-controllers in which the optimal wind power (P_{opt}) is compared with the actual generated power (P_{act}). The resulting error is handled by the first PI-controller, which defines the reference value of the DC-bus current for the next control loop. The actual DC-bus current is measured and compared with the pre-determined reference current; then, the mismatch is supervised using the second PI-controller. The controller generates the desired duty-cycle of the DC-DC boost converter under the different variabilities in the input side (the wind turbine side). Furthermore, a limiter is applied to the controller to handle the threshold value of the generator current.

The generated AC voltage is rectified through the three-phase uncontrolled rectifier where the average DC value of the rectifier output voltage, which at the same time is considered the input voltage (V_{in}) of the following DC-DC boost converter, is given by Eq. (15) where V_{peak} is the peak voltage value of the generated AC voltage.

$$V_{in} = \frac{3\sqrt{3}}{2\pi} V_{peak} \tag{15}$$

The input/output voltage and current relations for the DC-DC boost converter are given by the following relations where V_{out}, V_{in}, D, I_{out}, and I_{in} are the output voltage of the converter, the input voltage of the converter, the duty cycle, average output current, and the average input current, respectively [45]:

$$V_{out} = \frac{V_{in}}{1 - D} \tag{16}$$

$$I_{out} = (1 - D) I_{in} \tag{17}$$

From (16) and (17), the relation between output and the input resistance can be given by:

$$\frac{V_{out}}{I_{out}} = \frac{V_{in}}{(1-D)(1-D)I_{in}} = \frac{V_{in}}{(1-D)^2 I_{in}}$$

$$R_{out} = \frac{1}{(1-D)^2} R_{in} \tag{18}$$

$$R_{in} = (1-D)^2 R_{out}$$

From (18), it can be observed that by controlling the duty cycle of the DC-DC boost converter, the equivalent load side (output) resistance (R_{out}) will be changed and hence the input side resistance (R_{in}) will be changed. Therefore, the PMSG will be affected by the change of the resistance which affect the rotation speed of the PMSG. Therefore, by controlling the duty ratio, the rotation speed of the PMSG can be controlled and hence the MPPT can be accomplished.

2.2.3. *Control of the battery storage system*

In this study, a bidirectional buck-boost converter is employed with the proposed FLC for managing the power transferred between the DC-bus and battery and preserve the DC-bus voltage constant during the different instabilities to regulate its duty cycle and hence generate the suitable switching pulses. The bidirectional buck-boost converter's operating modes are primarily dependent on the difference between the generated power and the load demand power, which are translated into deviations of the actual DC-bus voltage level away from its desired (reference) value. The buck-boost converter allows regulating the DC-bus voltage during charging and discharging processes by operating in either bucking or boosting mode, respectively. The bucking (charging) mode is activated when the actual DC-bus voltage exceeds the reference DC-bus voltage. This mode usually takes place at higher wind speeds or higher solar radiation values, at which the total generated power becomes more significant than the load demand power. Hence, the battery controller starts decreasing the duty cycle until the actual DC-bus voltage matches the reference value; hence, the extra power is transferred from the DC-bus to the battery. Conversely, the boosting (discharging mode) occurs when the actual DC-bus voltage becomes lower

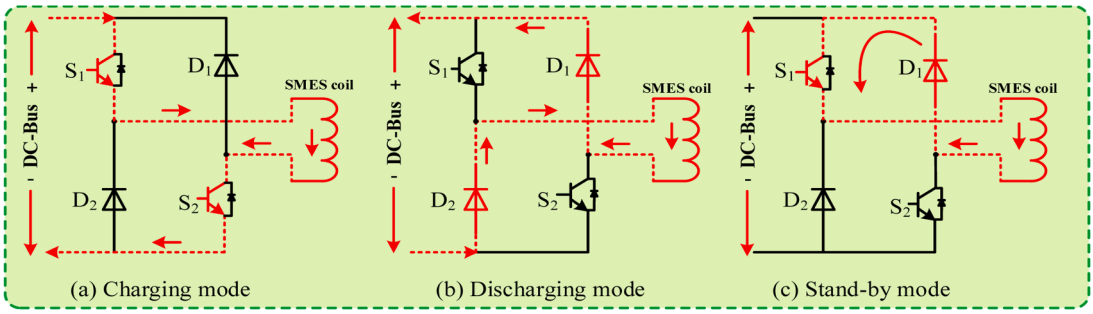

Fig. 12. Different operating modes of the SMES.

than the reference value. This mode typically occurs at lower wind speeds and low solar radiation values, at which the total generated power becomes insufficient to supply the load demand. So, the battery controller begins increasing the duty cycle of the buck-boost converter until the actual DC-bus voltage matches the reference value; hence, the stored power is transferred from the battery to DC-bus to overcome the occurring power deficiency.

The proposed FLC for the battery is designed with two inputs and one output. The first input is the change in the DC-bus voltage ($\Delta V_{dc,bat}$) which is the difference between the desired DC-bus voltage (V_{ref}) and the actual value ($V_{dc,bat}$). The second input is the actual battery current (I_{bat}) which reduces the necessity of calculations in case of using the change in voltage/current deviations as a second input. Besides, it facilitates monitoring the charging/discharging operation precisely and allows fast charging and discharging when required. The fuzzy output is the duty cycle (D_{bat}) required for generating the switching pulses for the buck-boost converter switches. Depending on ΔV_{dc} and I_{bat}, power is transferred to/from the battery according to the above-discussed explanation, which was translated into fuzzy rules. The fuzzification process uses triangular and special trapezoidal membership functions (the R and L functions). The membership functions of the first input are negative voltage margin (NVM), zero voltage margin (ZVM), and positive voltage margin (PVM), while for the second input, negative current margin (NCM) and positive current margin (PCM). For the output, the membership functions are small action (SA), no action (NA), and large action (LA). The inputs values are all normalized in [−1,1] while the output values are normalized in [0, 1] as shown in Fig. 11.

2.2.4. Control of the SMES system

The operation procedure of the SMES follows the same process as the battery regarding the DC-bus voltage deviation and the comparison between the generated and load powers. A two-quadrant chopper circuit is utilized to control the operation of the SMES. The direction of power transferred from/to the SMES to/from the DC-bus depends on the duty cycle value (D_{sm}), which is expressed in Eq. (19) where Vsm is the SMES voltage $V_{DC\text{-}bus}$ is DC-bus voltage [21].

$$V_{sm} = (1 - 2D_{sm})V_{DC-bus} \tag{19}$$

If D_{sm} is greater than zero and less than 0.5, power is transferred from the SMES to the DC-bus (discharging mode). If D_{sm} is greater than 0.5 and less than 1, power is transmitted from the DC-bus to the SMES (charging mode). The standby mode is activated when the duty cycle exactly equals 0.5. The SMES controller adjusts the duty cycle of the two-quadrant chopper depending on the difference between the total

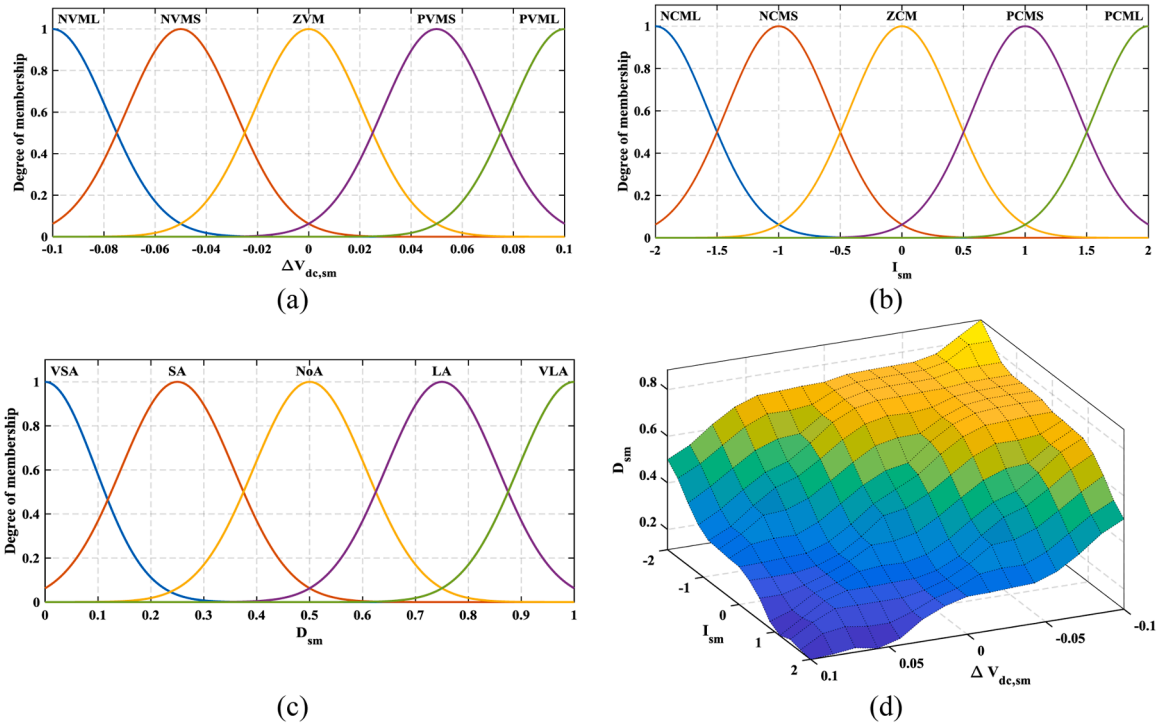

Fig. 13. Membership functions used for SMES control (a) Inpu-1, $\Delta V_{dc,sm}$ (p.u), (b) Input-2, I_{sm} (p.u), (c) The output D_{sm}, and (d) 3-D graph of inputs-output membership functions.

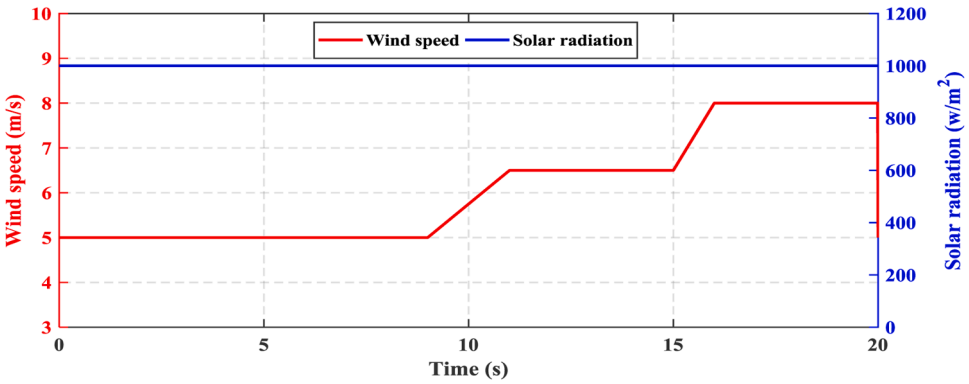

Fig. 14. The wind speed and solar irradiation variations of case-A.

generated power and load demand which are interpreted into deviations of the DC-bus voltage. For further explanation of SMES modes of operation, Fig. 12 displays the three operation modes describing the switching sequence in the two-quadrant chopper circuit. The charging mode is attained by employing positive voltage across the SMES coil via switching-on S_1 and S_2 as exhibited in Fig. 12 a; in this mode, the power is transferred from the DC-bus MG to the SMES system. The discharging mode (Fig. 12-b) is achieved by applying a negative voltage across the SMES coil throughout D_1 and D_2; hence, the power is transferred from the SMES to the DC-bus MG. In the standby mode indicated in Fig. 12 c, two different freewheeling paths are possible through (S_1 and D_1) or (S_2 and D_2), where the voltage across the SMES coil becomes zero and the power circulates in one of the freewheeling paths, hence; no power transfer. The proposed FLC for the SMES, which aims at defining and moderating these three modes, is designed with two inputs and one output, as illustrated in Fig. 8. Similar to the FLC applied for the battery, the first input is the change in the DC-bus voltage ($\Delta V_{dc,sm}$), and the second input is the actual SMES current (I_{sm}), while the fuzzy output is the duty cycle (D_{sm}) needed for the bi-directional dc-dc converter. The defined rules permit the quick charging and discharging process and enable supervising the different operation modes accurately; the features greatly enhance the controller robustness during the different instabilities.

The fuzzification and defuzzification procedures use Gaussian functions. The membership functions of the first input are negative voltage margin large (NVML), negative voltage margin small (NVMS), zero voltage margin (ZVM), positive voltage margin small (PVMS), and positive voltage margin large (PVML). The second input membership functions are similar to the first input ones; the letter V for voltage is replaced by C for current. For the output, the membership functions are very small action (VSA), small action (SA), no action (NoA), large action (LA), and very large action (VLA). The first input, second input, and output values are normalized in [−0.1, 0.1], [−2, 2], and [−1,1], respectively as shown in Fig. 13.

2.2.5. *Control of the prime inverter*

It is essential to alleviate the load power in terms of voltage magnitude and frequency throughout the inverter control circuit. There are two main classifications of controlling the inverter in which each classification includes distinct schemes of control; the first is the pulse width modulation feed forward scheme which includes the sinusoidal pulse-width modulation (SPWM) [46]. The second scheme is the pulse width modulation feedback which includes the hysteresis current control and the space vector pulse-width modulation. Due to the various inverter control techniques, there are control methods in which the dq-axis components can be employed to obtain the modulation index. On the other side, other control approaches are achieved by directly obtaining the controlled modulation index. As this work's primary focus is to enhance the stability and power quality performance of PV/Wind DC-bus MGs using battery or SMES systems based FLC, a proposed straightforward inverter control technique based-SPWM is used to control the load voltage and frequency during balanced and unbalanced loading events. In this technique, a high-frequency carrier signal is compared with three unit-vector sinusoidal modulating signals shifted by 120 ° and has the required output/load frequency. The gating signal for a particular phase results from comparing the carrier and the modulating signal corresponding to that phase. The relationship between the input DC voltage and the output line-voltage is given by Eq. (20) [46]:

$$V_{line} = m \times 0.6124\ V_{dc-bus} \tag{20}$$

The magnitude of the inverter output voltage depends on the amplitude of the modulation index (m) and the value of input DC voltage. From Eq. (20), the inverter's output voltage depends on the modulation index and the input DC voltage, which must be maintained constant. Hence, the required AC voltage in the output determines the necessary modulation index. In this work, the prime inverter can be controlled to supply either a balanced or unbalanced load. For balanced loading conditions, the same modulation index is employed for the three phases. For unbalanced loading conditions, using the same modulation index for all phases makes the control unacceptable since it produces different (unequal) output voltage for all phases. In order to overcome this problem, the study proposes a variable modulation index control technique used to control each phase separately, as shown in the prime inverter control part in Fig. 8. From the figure, it can be seen that the input of each PI-controller is the voltage deviation between the reference rms phase voltage and the actual rms phase voltage. The PI-controllers handle the mismatch that occurs in phase voltages then generate the modulating signal amplitude for each phase, which is then entered to a limiter or a saturation block to limit its value below the unity. The required firing pulses for each inverter switch are generated using the proposed variable modulation index in which the three sinusoidal modulating signals are generated for each phase with different amplitude according to the output of the corresponding PI-controller.

3. Results and discussion

This section presents the main findings obtained from the investigation in which five different assessments were evaluated. Based on the main aims of this study, the performance of the DC-bus MG integrating batteries and SMES systems has been examined, compared, and analyzed under the same operation circumstances. For all results, it should be remarked that the WT is connected to the MG after 5 s since it requires this period for the produced voltage to reach its steady state. Therefore, during the first five seconds, loads are energized from the PV system and batteries/SMES if needed.

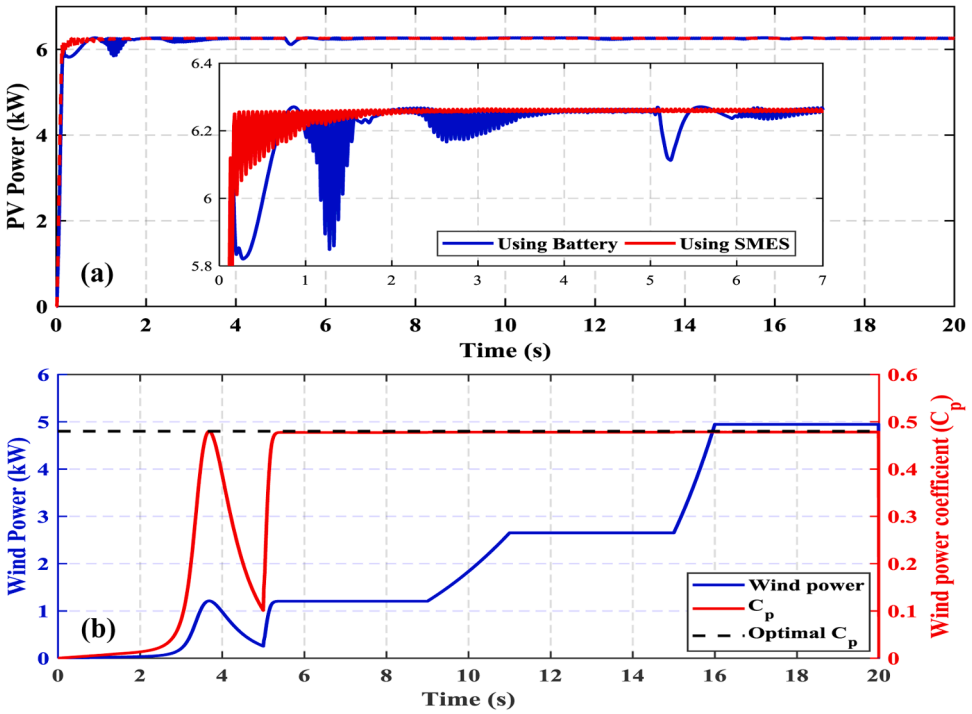

Fig. 15. The generated power during case-A (a) PV power (b) wind power and its coefficient.

3.1. Case-A: variable wind speed, constant radiation and load

In this case, the system was examined under variable wind speed considering constant solar radiation, as shown in Fig. 14, while the load demand was kept constant at 7.26 kW. The MPPT control approaches successfully achieved the aimed target by attaining the maximum available power from the wind and solar energies as verified from the PV power and the wind power coefficient indicated in Fig. 15. Besides attaining the maximum power, similar FLC approaches were applied to both battery and SMES systems to produce a more reasonable comparison. As evident from the produced PV power shown in Fig. 15 a, the SMES system has improved the response of the PV power during the climatic changes and the WT connection more smoothly than the battery, while the wind power remained the same using both battery and SMES systems as shown in Fig. 15 b. Moreover, the load power was enhanced in terms of response time and overshoot at instants of disturbances using the SMES system compared to the battery, as shown in Fig. 16 a. This enhancement in the load power verifies the control approaches' ability to sustain the DC-bus voltage, the load rms voltage constant during the examined variations as presented in Fig. 16 b, c in which the SMES has superior performance over the battery. Besides, Fig. 16 d, e validate the effectiveness of the inverter controller to uphold the load voltage/frequency constant during climatic conflicts. These figures show that the instantaneous load voltage using SMES is much better than the instantaneous load voltage using the battery.

Power-sharing and DC-bus power are crucial issues that must be discussed and analyzed using the proposed control approaches. Regardless of the generated power variations or load disturbances, the DC-bus power must be leveled all the time. Fig. 17 (a, b) indicate the power-sharing among all system components using battery and SMES, respectively. From the figures, it can be noticed that the PV power is flattened magnificently using the SMES compared to the battery. The figures also indicate that the DC-bus power was kept flattened regardless of the occurring disturbances with superior performance of SMES over the battery. In Fig. 17 a, the SMES charges (positive sign) and discharges (negative sign) are based on the system status. The discharge mode is activated when the DC-bus voltage is lower than the desired value and the SMES has sufficient energy. In contrast, the SMES receives power from the system when the DC-bus voltage is higher than the desired value. Similarly for the battery, the control approach is designed, but the positive sign means that the battery discharges power to the MG and the negative sign means that the battery receives power from the MG, as indicated in Fig. 17 b. The behaviors of both battery and SMES are offered in Fig. 17 (c, d) indicate the charging and discharging procedure in terms of currents, energy, and SOC.

3.2. Case-B: variable radiation, constant wind speed and load

The performance system is examined in this case under variable solar radiation and constant wind speed as offered in Fig. 18, assuming constant load demand of 4.84 kW. The optimal operation of the wind and PV systems was successfully achieved, which is reflected in power generated from the WT and PV systems displayed in Fig. 19. Since preserving the load power is considered one of the most vital challenges in MG systems, it is essential to distribute the power to the consumers smoothly. The proposed FLC approach applied for the SMES system is more effective and robust than using the battery to flatten the load power, as shown in Fig. 20. In the case of using the SMES, the load power profile is smoothed out successfully, while for the battery, it has overshoots and undershoots at the instants of the starting, changing the solar radiation and the WT connection.

The behavior of the DC-bus voltage is presented in Fig. 21 a, in which, in the case of using SMES, it has less rise time; thus, it reaches the steady-state more rapidly than the battery. In addition, the transient events during disturbances are profitably mitigated using the SMES, where the maximum value reaches 700 V (the reference value). Meanwhile, for battery, the maximum overshoot value reaches 768 V. The enhancement in the DC-bus voltage is directly reflected on the load rms voltage as shown in Fig. 21 b, where the rise time in case of using a battery is more than using SMES. The maximum overshoot reaches 224.6 V when using the battery while it equals 219.9 V using the SMES, which verifies the effectiveness of the proposed FLC approaches and the superiority of the SMES over the battery. The superiority of the SMES can also be noticed through the instantaneous load voltage, as shown in

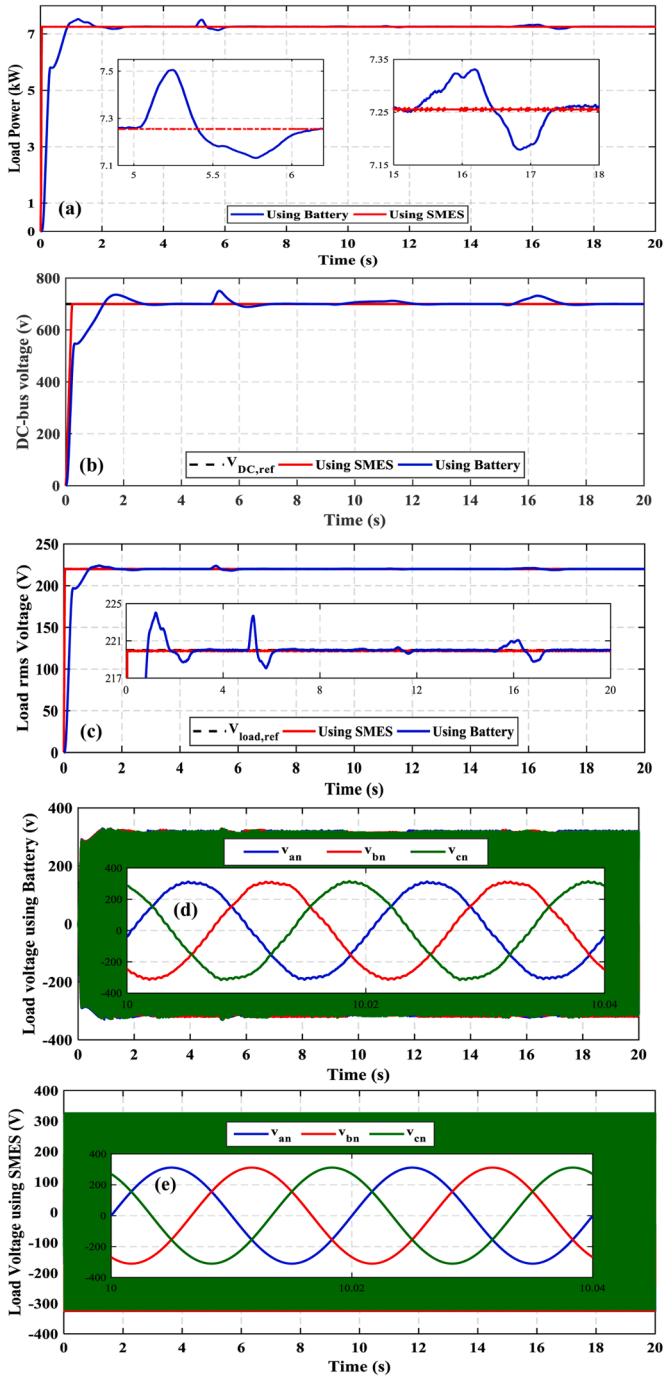

Fig. 16. Results of case-A (a) load power, (b) DC-bus voltage, (c) load rms voltage, (d) instantaneous load voltage using the battery, and (e) instantaneous load voltage using SMES.

Fig. 21 c, d, where the load voltage response using SMES is smoother than using the battery.

The power-sharing among all system components in the SMES and battery is shown in Fig. 22 a, b, respectively. The generated power from both PV and wind systems have followed the climatic changes (i.e., irradiance and wind speed) according to the proposed MPPT techniques. In Fig. 22 a, the SMES utilization leads to a more smoothed DC-bus power than the battery, regardless of the occurring variations. Moreover, the settling time is minimal, leading to a swift response to reach the steady-state. The SMES charges power (positive sign) when the total generated power is greater than the load power, as shown in the period between 11 and 15 s. Meanwhile, the SMES discharges (negative sign)

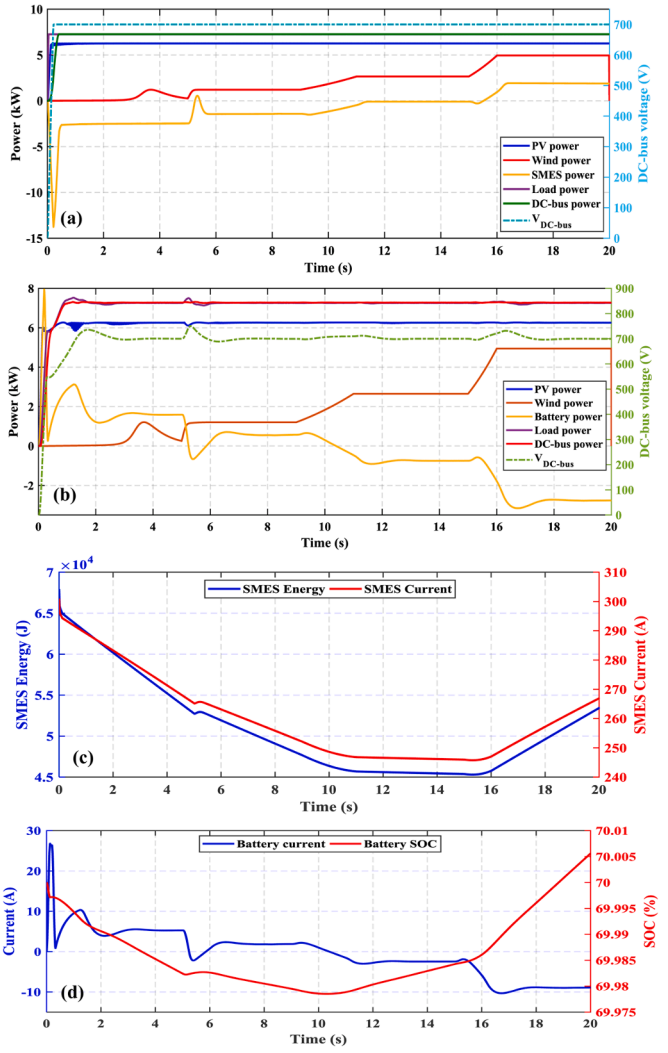

Fig. 17. Power sharing and storage devices' performance during case-A (a, c) SMES and (b, d) battery.

when the load demand becomes more remarkable than the total generated power, as shown in the period between 1 and 5 s. Similarly, for the battery, the battery charges (negative sign) when the generator power is more significant than load power, as transpired from 10 to 20 s. Also, the battery discharges (positive sign) when the load power become higher than generated power as in the (0–5 s) period. The response of the SMES shows little ripples and settles down quickly compared to the battery. The SMES dynamic behavior is shown in Fig. 22 c in terms of SMES current and the energy varying according to the operation mode. Meanwhile, Fig. 22 d offers the battery SOC and battery current, which go up and down according to the system status that defines the battery mode of operation.

3.3. Case-C: variable load, constant radiation, and constant wind speed

In this case, the load power is increased in an ascending behavior. For the first nine seconds, the load demand was 4.84 kW, then risen to 8.47 kW (9 to 15 s), and finally increased to 10.54 kW (15 to 20 s). Simultaneously, solar radiation and wind speed are presumed unchanged at 1 kw/m^2 and 6.5 m/s, respectively. Fig. 23 highlights the beneficial impact of the SMES over the batteries in smoothing the PV power during the load variation instants. Besides, the behavior of the wind power persisted the same using both battery and SMES. Similar to the previous cases, Fig. 24 exemplifies the power-sharing in the system

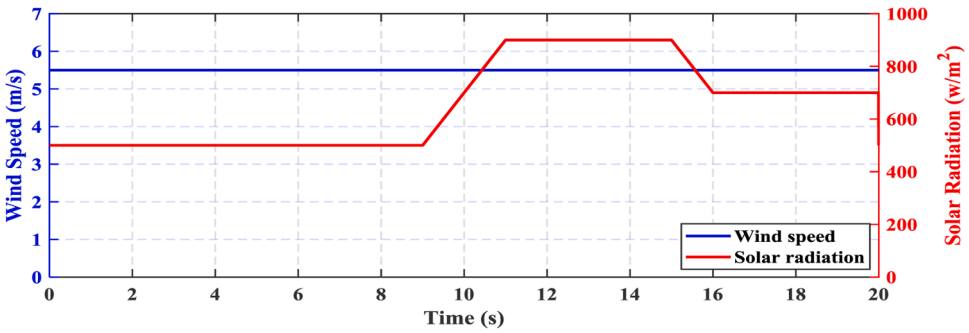

Fig. 18. The wind speed and solar irradiation profiles during case-B.

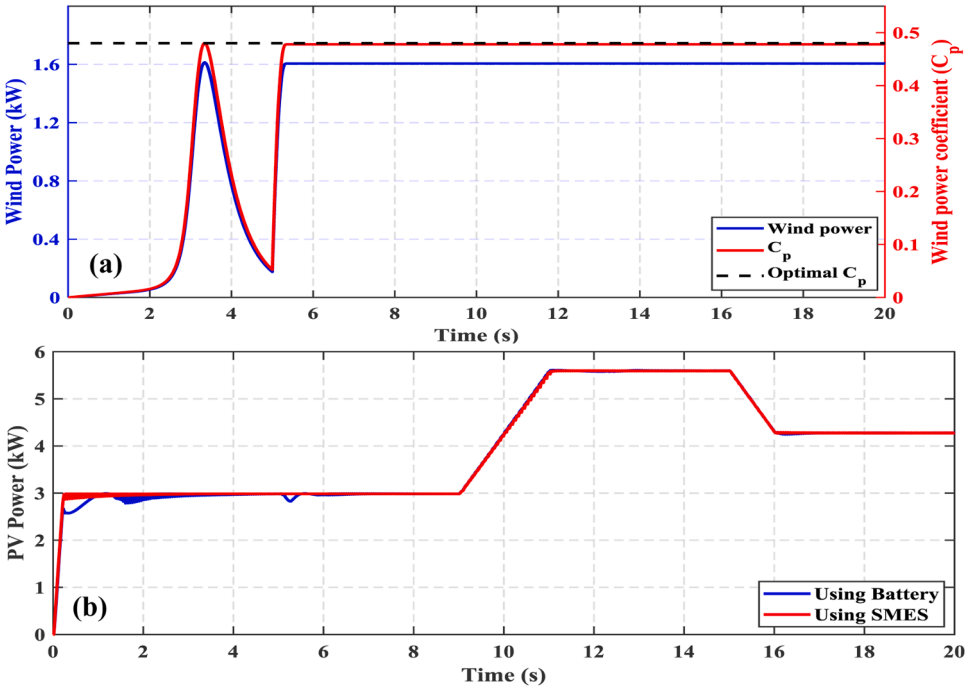

Fig. 19. The generated power during case-B (a) wind power (b) PV power.

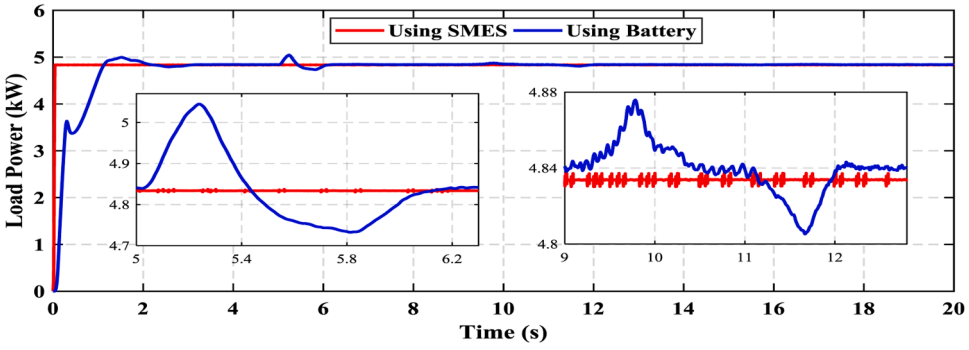

Fig. 20. Load power during case-B.

from which the efficacy of the proposed control approaches using both battery and SMES is verified. From the figure, the battery and SMES kept the extra power (0–9 s) when the generation side fulfilled the load. However, when the load increased by 75% and 117%, respectively, both energy storage devices started discharging the power to fulfill the load requirements and uphold the system steady. The performance of both battery and SMES in terms of currents, energy, and SOC is presented in Fig. 25.

Moreover, the proposed FLC approaches, applied for battery and SMES controllers, efficiently maintained the DC-bus and load voltages, as shown in Fig. 26 (a, b). From Fig. 26 (a, b), it can be realized that both DC-bus and load rms voltages are practically preserved constantly during the investigation time using the SMES, while for the battery, both voltages have overshoot and undershoot. The disparities between

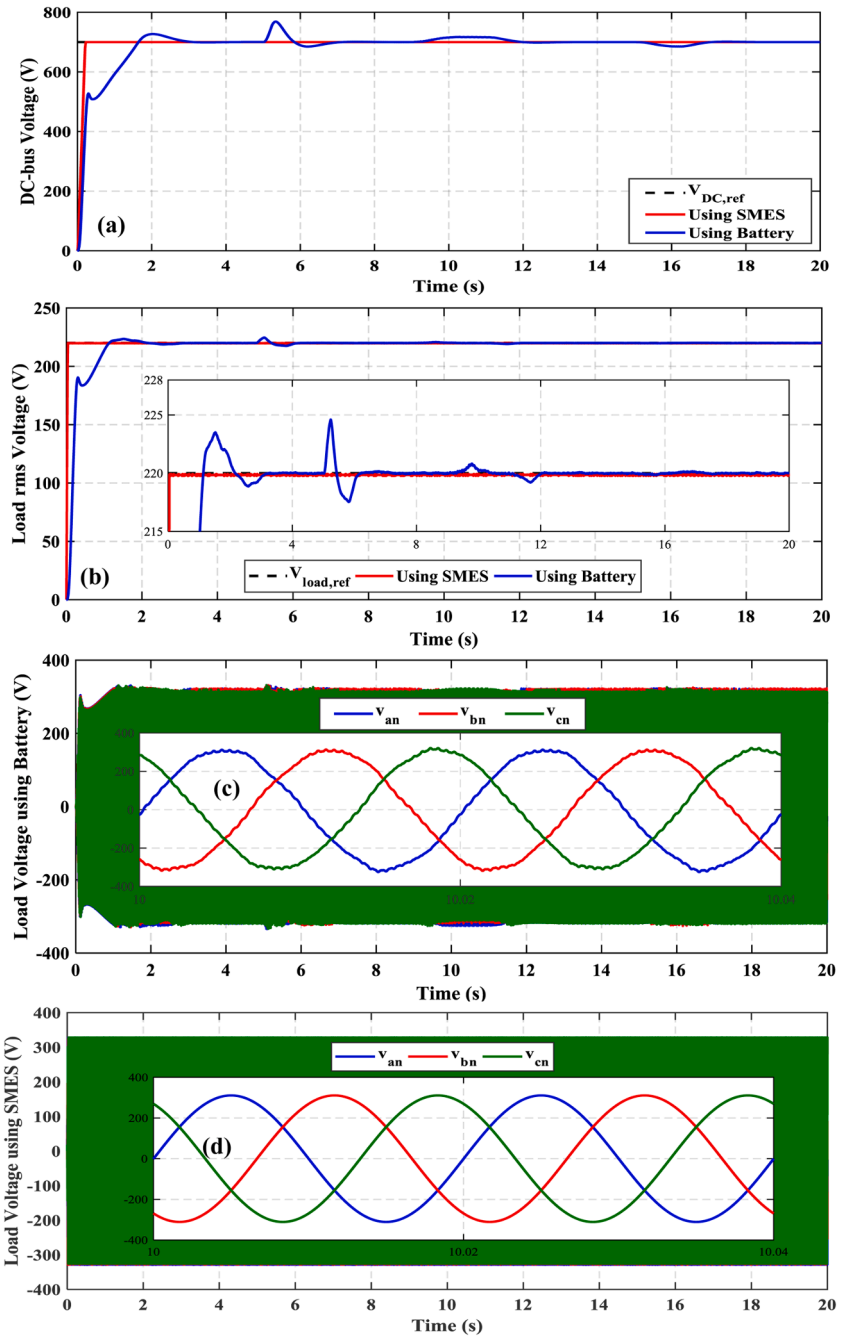

Fig. 21. Results of case-B (a) DC-bus voltage, (b) load rms voltage, (c) instantaneous load voltage using a battery, and (d) instantaneous load voltage using SMES.

battery and SMES can also be detectable through the instantaneous load voltage envelope shown in Fig. 26 (c, d). Moreover, the enhancement of the DC-bus voltage and the load rms voltage is reflected in smoothing the load power as displayed in Fig. 26 e, in which the SMES efficiently smoothed out the load power over the battery. In conclusion, it can be realized that the response time and the potential to mitigate the load instabilities using the SMES is exceptional compared to the battery.

3.4. Case-D: wind gust with rapid shadow and constant load

In this case, a wind gust and rapid shadow were considered concurrently while the load power remained unchanged at 4.84-kW as depicted in Fig. 27. The SMES performance showed a magnificent behavior to sustain the DC-bus and the load rms voltages constant over the battery as shown in Fig. 28. This can be verified from the impressive response time of the SMES at starting and instants of disturbances and the flatness of both DC-bus and load voltages. The improvement of voltages directly impacts the load power, as portrayed in Fig. 29 a, in which the SMES superbly flattened the load power during all disturbances over the battery. Furthermore, the power-sharing during the wind speed and solar radiation disturbances using the battery and SMES are displayed in Fig. 29 b, c, in which the proposed control methods profitably moderated the power exchange in the system. The behavior of both the battery and SMES is shown in Fig. 29 d, e, in which the energy storage elements discharged power to supply the load during the first 10 s where the load power is greater than the total generated power. During the wind gust and the rapid decrease in solar radiation, both battery and SMES controllers competently handled the disturbance by adjusting the duty cycle to preserve the load nourishment.

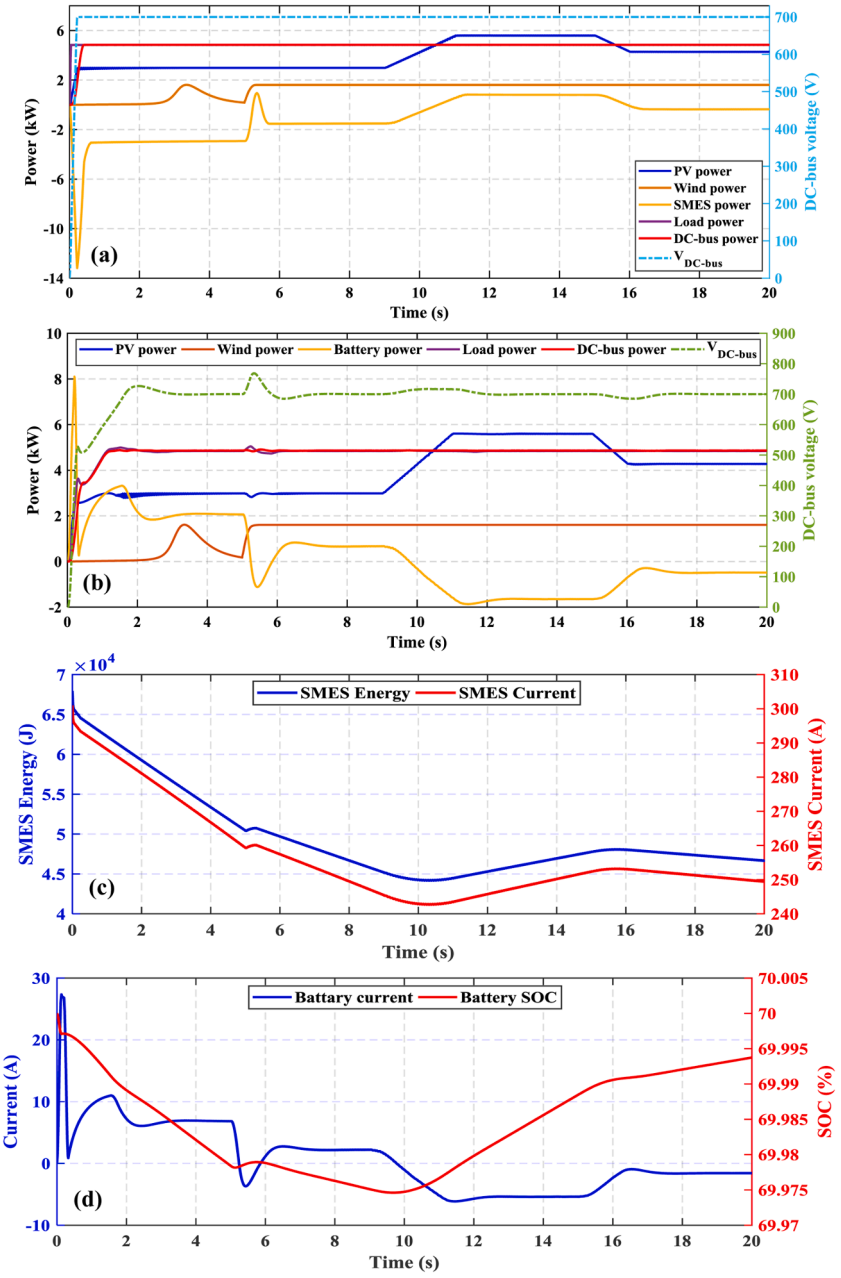

Fig. 22. Power sharing and storage devices' performance during case-B (a, c) SMES and (b, d) battery.

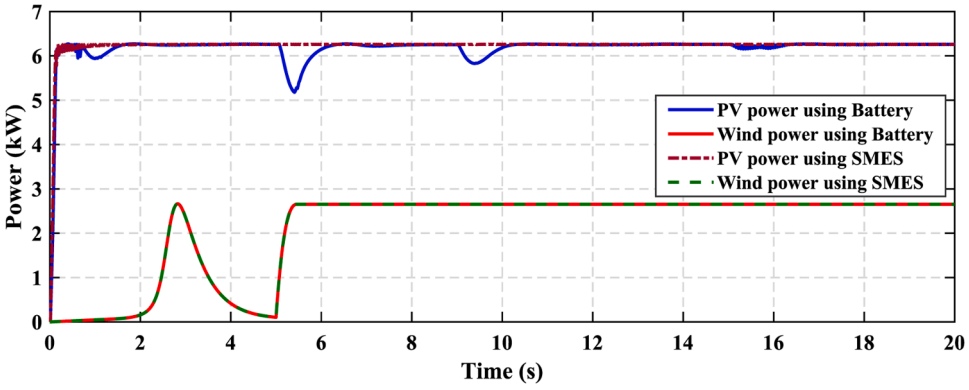

Fig. 23. PV and wind powers using both battery and SMES.

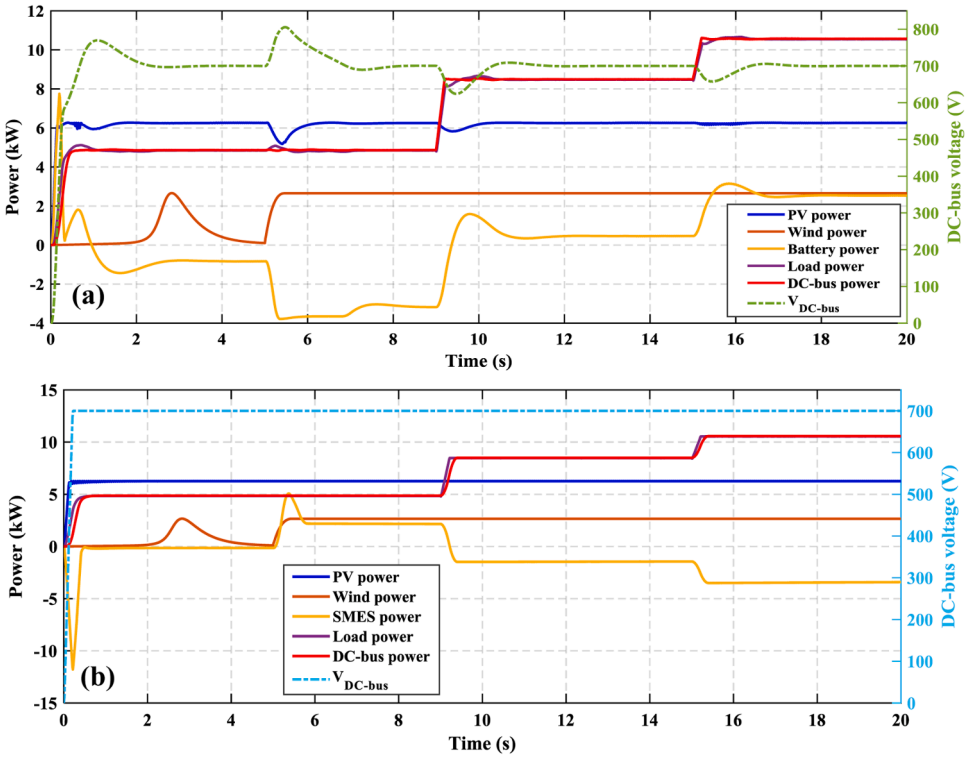

Fig. 24. Power sharing during case-C (a) using the battery (b) using SMES.

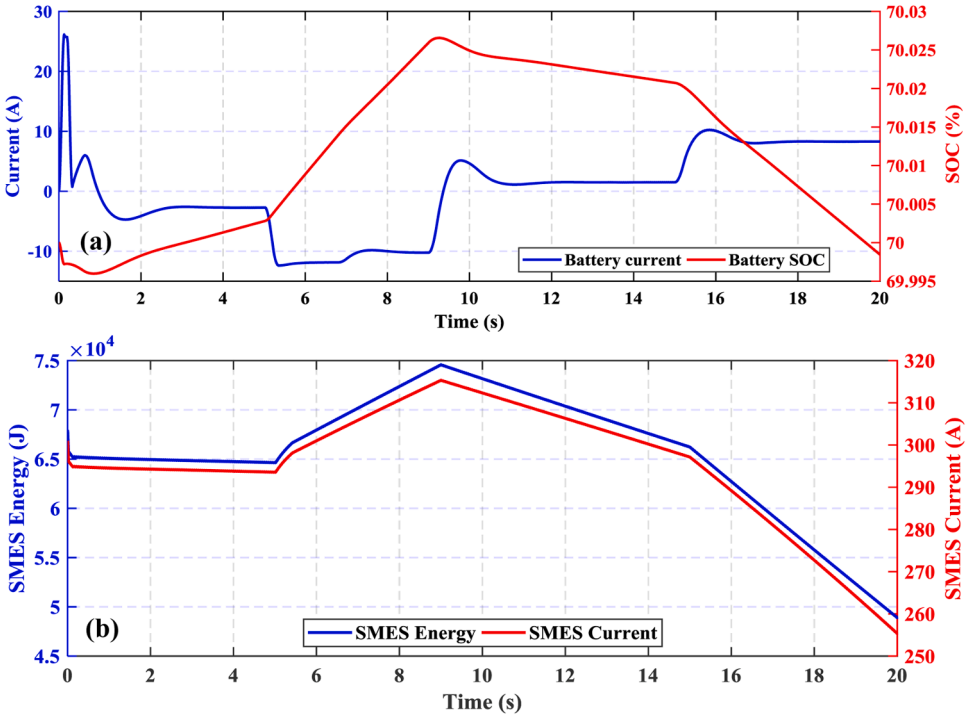

Fig. 25. Performance of the a) battery, b) SMES, during case-C.

3.5. Comparison among all cases

To clarify the different disparities between the SMES and battery systems on the DC-bus MG performance, Table 6 summarizes a comprehensive comparison among the previous four assessments in the presence of SMES and battery systems. The comparison includes the peak overshoot/undershoot of voltages and load power and the corresponding rise and settling times. From the table, it can be recognized that the SMES magnificently mitigated the DC-bus and load voltages to the desired references values besides smoothing out the load power during all assessment tests. Fig. 30 shows a comparison between the peak overshoot/undershoot values in the DC-bus voltage using the two

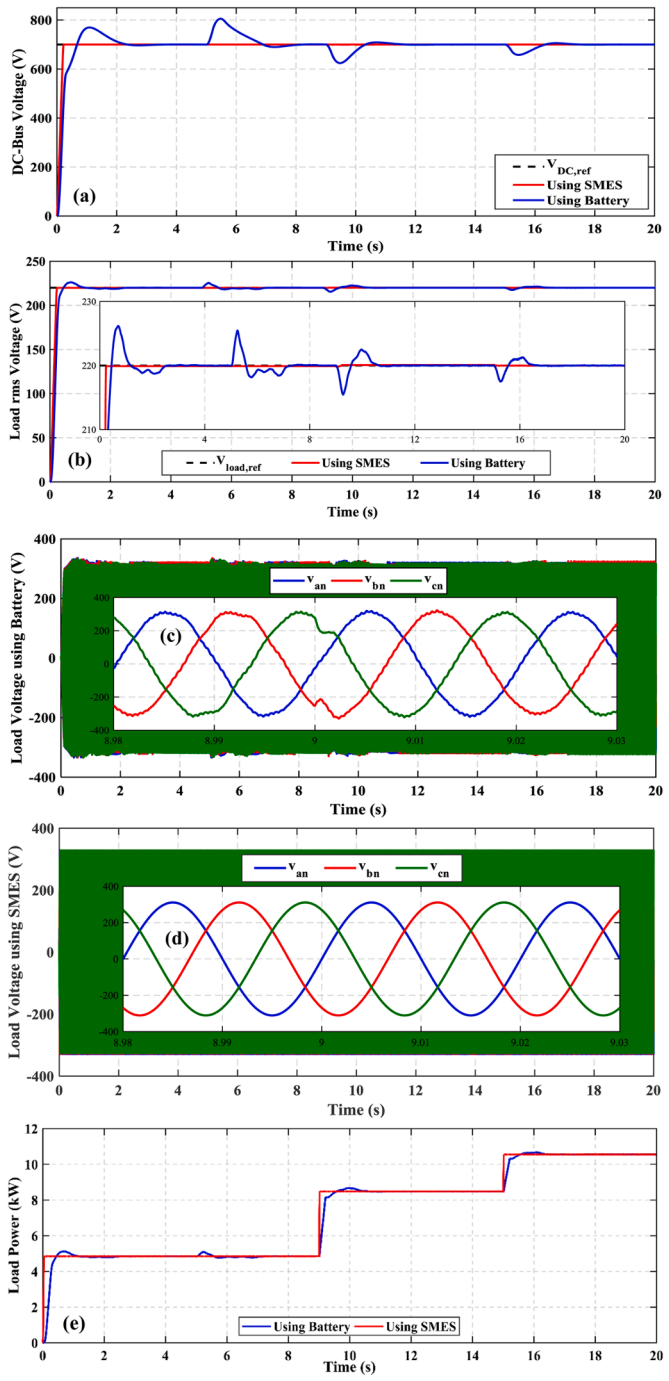

Fig. 26. Results of case-C (a) DC-bus voltage (b) load rms voltage (c) instantaneous load voltage using the battery (d) instantaneous load voltage using SMES, (e) load power.

ESTs in which the superior performance of the SMES can be recognized. Moreover, the SMES response time represented in both rise and settling times is extremely rapid compared to the battery system. Conversely, the BSS also successfully maintained the DC-bus voltage, load voltages, and load power constant but with a sluggish response with high peak overshoot/undershoot values during the different disturbances.

3.6. Unbalanced loading event

To demonstrate the efficacy of the proposed inverter control technique during the unbalanced loading events, simulations were accomplished for both battery and SMES systems. The system began delivering electricity to a balanced three-phase load for the first 3 s even as the load came to be unbalanced past 3 s. The balanced three-phase load has changed from 30 Ω/phase to 32 Ω/phase, 35 Ω/phase, and 30 Ω/phase for phases a, b, and c respectively, which means an unbalance in both phases a, and b. The proposed inverter control technique generated different modulation indices during the unbalanced loading event to keep the load voltage rms value fixed at 220 V (the desired value) using both the battery and the SMES system as shown in Fig. 31 (a and b), respectively. Besides, the instantaneous load voltage using battery and SMES is also shown in Fig. 31 (c and d). The current and power distribution among the phases using battery and SMES are shown in Fig. 31 (e and f) and Fig. 31 (g and h), respectively. From Fig. 31 (a and b) to (c and d), it can be recognized that the inverter controller efficiently managed to preserve the load voltage and frequency constant during the sudden load unbalance in phases a and b using both ESTs. Also, the phase-voltage deviation that occurred at the unbalance instant ($t = 3$ s) can be neglected due to its tiny value and thanks to the control technique potency, which sent the voltage back to the desired value in a very quick time.

3.7. Comparison with relative research works

In order to evaluate the performance characteristic and clarify the effectiveness of the proposed work, Table 7 summarizes a comparison among the proposed study and relative research works. The majority of studies gave more attention to utilizing the PI controller to regulate the operation of either batteries or SMES while few works implemented advanced controllers such as FLC or MPC for the control action. Besides, the extreme variation of either wind speed or solar radiation was not examined in most studies. Furthermore, the unbalanced loading event was not investigated or mitigated in all of the addressed research studies.

4. Conclusions

This study discussed a comparative analysis between the integration of battery storage and SMES systems into a hybrid PV/wind DC-bus MG considering normal and extreme climatical and load variations. Each PV and wind system was outfitted with a distinct maximum power point tracking technique to acquire the maximum possible power from solar and wind energies, respectively. A developed control approach in a fuzzy environment was applied for both battery and SMES systems to regulate the DC-bus voltage and supervise the power exchange among system's elements during the different circumstances of wind speed, solar radiation, and load demand. Moreover, to serve the consumers with a high-quality power supply, the prime inverter was supplied with a variable modulation index controller, preserving the load voltage and frequency constant during the different instabilities. The PV unit, the WT, and the energy storage element are all connected at the DC-bus. The power conveyed between the DC-bus and the battery, or the SMES coil was regulated through the proposed FLC of the charge/discharge circuit. The FLC was constructed to enable the energy storage device to swiftly charge/discharge power to reimburse the voltage and line power fluctuation at the DC-bus. The proposed FLC approach was constructed based on quantifying change in the DC-bus voltage and measuring the actual current of both battery and SMES systems. These currents were utilized directly in the FLC, decreasing the necessary estimations, computations, and control system complications. Extensive simulations were obtained by addressing five different test cases, considering the different load demand variations, including balanced and unbalanced loading events and normal and extreme climatic variations. In line with the obtained results, the key findings can be emphasized as follows:

- The maximum power point tracking technique of both PV and wind systems efficiently extracted the maximum potential power during the regular and extreme climatic variations.

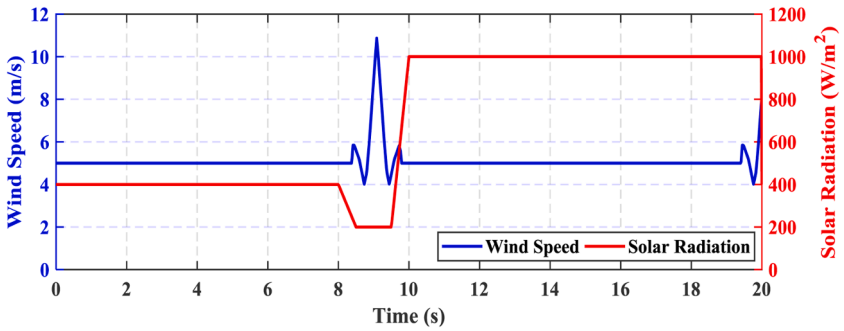

Fig. 27. Wind speed and solar radiation profile during case-D.

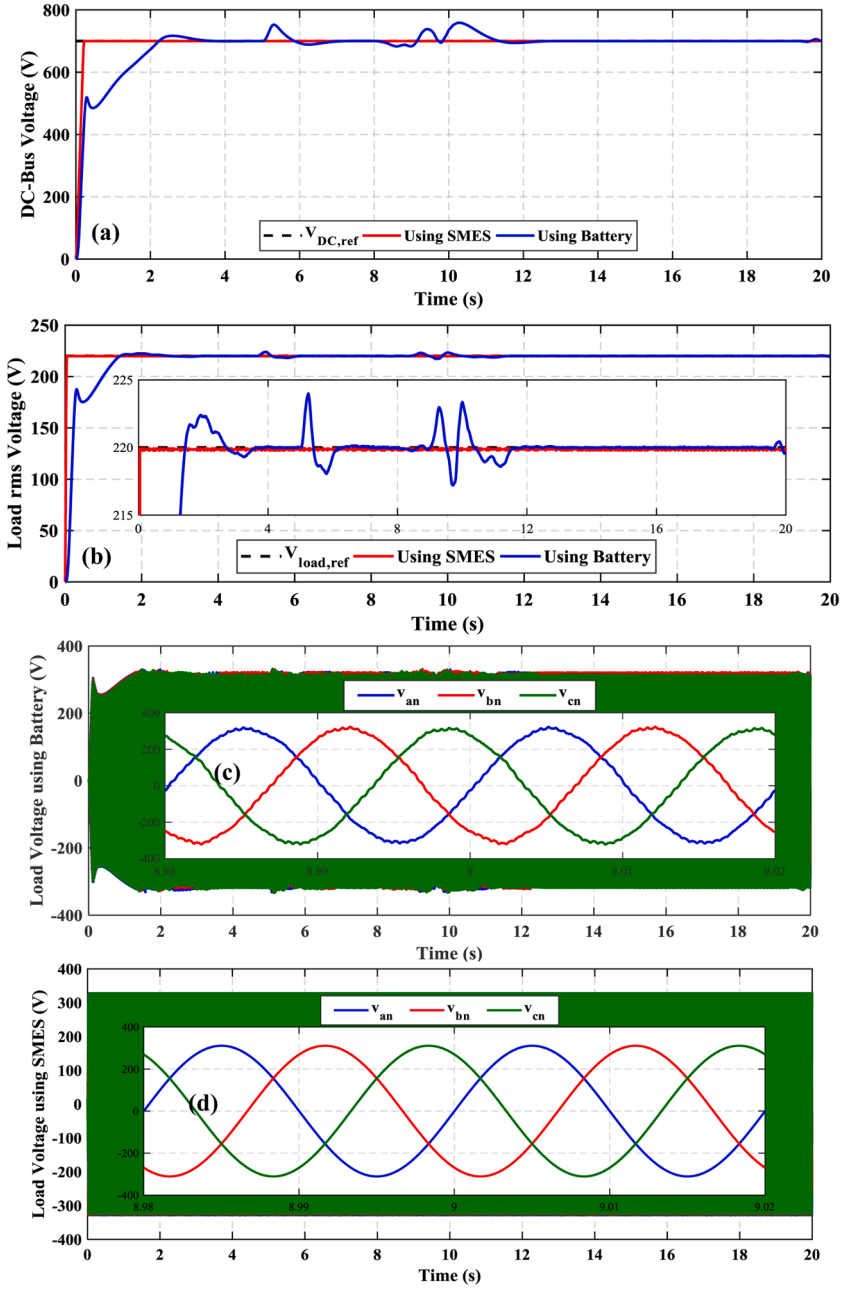

Fig. 28. Results of case-D (a) DC-bus voltage (b) load rms voltage (c) instantaneous load voltage using the battery (d) instantaneous load voltage using SMES.

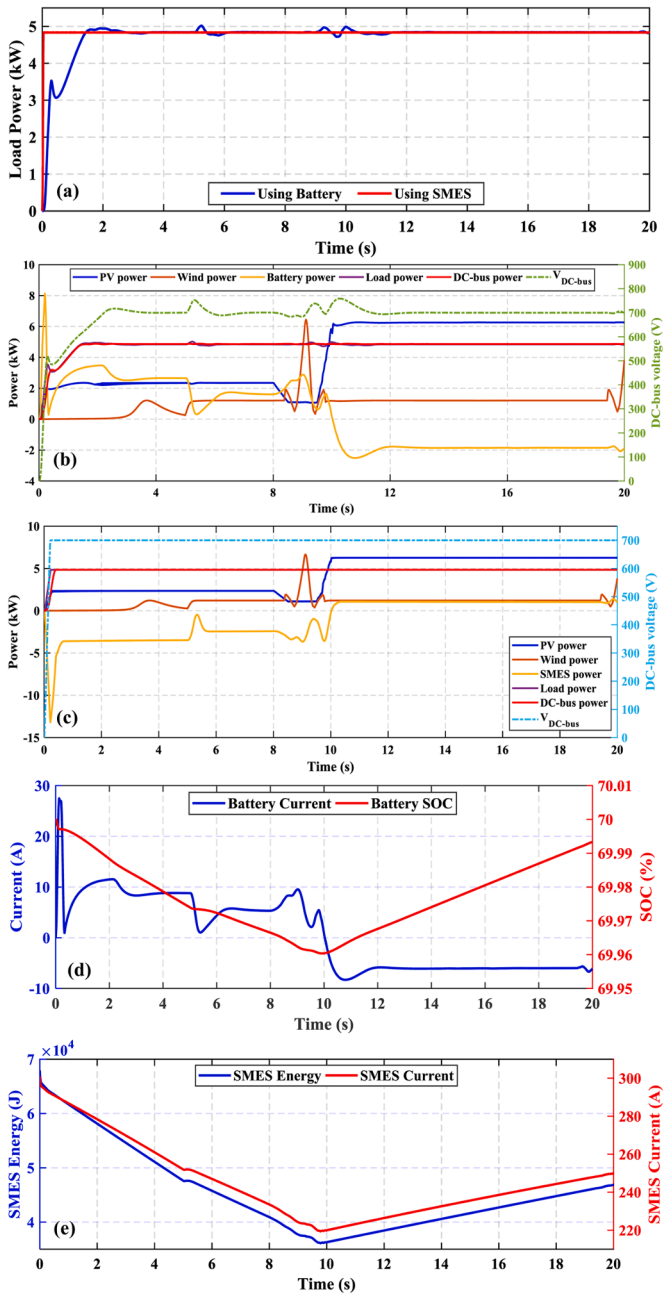

Fig. 29. Results of case-D (a) load power (b) power-sharing using battery (c) power-sharing using SMES (d) battery behavior, (e) SMES behavior.

- The proposed FLC approaches for battery and SMES systems constructively mitigated the DC-bus voltage and enhanced the power exchange between the generation and load sides during the different climatical and load fluctuations.
- The variable modulation index technique, which was proposed to control the prime inverter, profitably preserved the load voltage/frequency and consequently the load power constant and smooth during balanced and unbalanced loading events.
- With the proposed FLC approach, the SMES system proved a superior performance over the battery system in response time, voltages over- and undershoot limits, instantaneous load voltage profile, and load power smoothness. The SMES system succeeded in swiftly charging/discharging the stored energy during normal and high wind fluctuation, solar radiation, and random load instabilities, which assisted in adjusting the DC-bus voltage to the appropriate standard boundaries. The SMES system also managed to mitigate the active power exchange between the generation and consumers sides. Moreover, the SMES system directly impacted the flattening out the PV power during the examined disturbances over the battery. Ultimately, the SMES system offered a decent reaction throughout charging/discharging/standby operation modes which validates the usefulness of the proposed control approach.

Table 6
Comparison among the four assessments using SMES and battery systems.

Case	Item/ Reference	Parameter	Battery	SMES
A	DC-bus voltage (Ref. = 700 V)	Peak (overshoot-undershoot)	(50.4 – 11) V	(0.1 – 0.2) V
		(Rise time-settling time)	(0.875 – 2.31) s	(0.159 – 0.218) s
	Load voltage (Ref. = 220 V)	Peak (overshoot-undershoot)	(4 – 1.7) V	(0.05 – 0.1) V
		(Rise time-settling time)	(0.372 – 0.896) s	(0.027 – 0.039) s
	Load power (Ref. = 7.26 kW)	Peak (overshoot-undershoot)	(0.267 – 0.128) kW	(0.002 – 0.008) kW
		(Rise time-settling time)	(0.563 –1.89) s	(0.02 – 0.039) s
B	DC-bus voltage (Ref. = 700 V)	Peak (overshoot-undershoot)	(68.4 – 15.1) V	(0.05 – 0.2) V
		(Rise time-settling time)	(1.154– 3.127) s	(0.1598 – 0.2332) s
	Load voltage (Ref. = 220 V)	Peak (overshoot-undershoot)	(4.6 – 2.4) V	(0.02 – 0.1) V
		(Rise time-settling time)	(0.6731– 1.133) s	(0.1598 – 0.2332) s
	Load power (Ref. = 4.84 kW)	Peak (overshoot-undershoot)	(0.205 – 0.107) kW	(0.003 – 0.009) kW
		(Rise time-settling time)	(0.8142 – 2.243) s	(0.02 – 0.039) s
C	DC-bus voltage (Ref. = 700 V)	Peak (overshoot-undershoot)	(105.5 – 75.8) V	(0.08 – 0.2) V
		(Rise time-settling time)	(0.403 –2.337) s	(0.159 – 0.22) s
	Load voltage (Ref. = 220 V)	Peak (overshoot-undershoot)	(6.2 – 4.4 V	(0.1 – 0.1) V
		(Rise time-settling time)	(0.188 – 1.166) s	(0.16 – 0.24) s
	Load power Ref. = 4.84 kW, 8.47 kW, and 10.54 kW	Peak (overshoot-undershoot)	(0.281 – 0.075) kW, (0.196 – 0.006) kW, (0.13 – 0.001) kW	(0.004– 0.001) kW, (0.011 – 0.006) kW, (0.001– 0.0) kW
		(Rise time-settling time)	(0.203 – 0.961) s, (0.749- 1.08) s, (0.08 – 0.54) s	(0.02 – 0.04) s, (0.005 – 0.02) s, (0.01 – 0.02) s
D	DC-bus voltage (Ref. = 700 V)	Peak (overshoot-undershoot)	(58.7 – 17.4) V	(0.0 – 0.2) V
		(Rise time-settling time)	(1.515 – 2.828) s	(0.16 – 0.218) s
	Load voltage (Ref. = 220 V)	Peak (overshoot-undershoot)	(4 – 2.7) V	(0.05 – 0.2) V
		(Rise time-settling time)	(0.863 – 1.458) s	(0.027 – 0.04) s
	Load power (Ref. = 4.84 kW)	Peak (overshoot-undershoot)	(0.117 – 0.12) kW	(0.001 – 0.01) kW
		(Rise time-settling time)	(1.04 – 2.106) s	(0.021 – 0.04) s

It is worth mentioning that the superior performance of the SMES over the battery and its physical implementation still has several constraints due to the cost limitations, especially in its cryogenic system. Temporarily, investigations are still being developed to reduce the SMES cost to expand its power system applications implementation. The outlook of the work is directed towards implementing hybrid energy

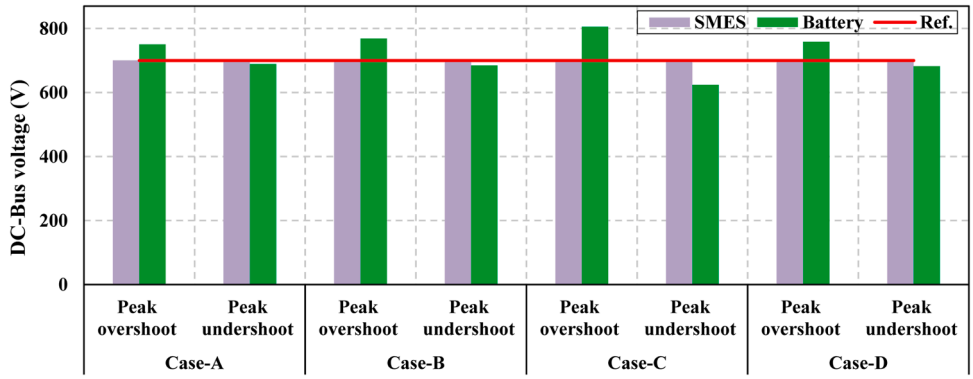

Fig. 30. Comparison between the DC-bus voltage during all cases using battery and SMES systems.

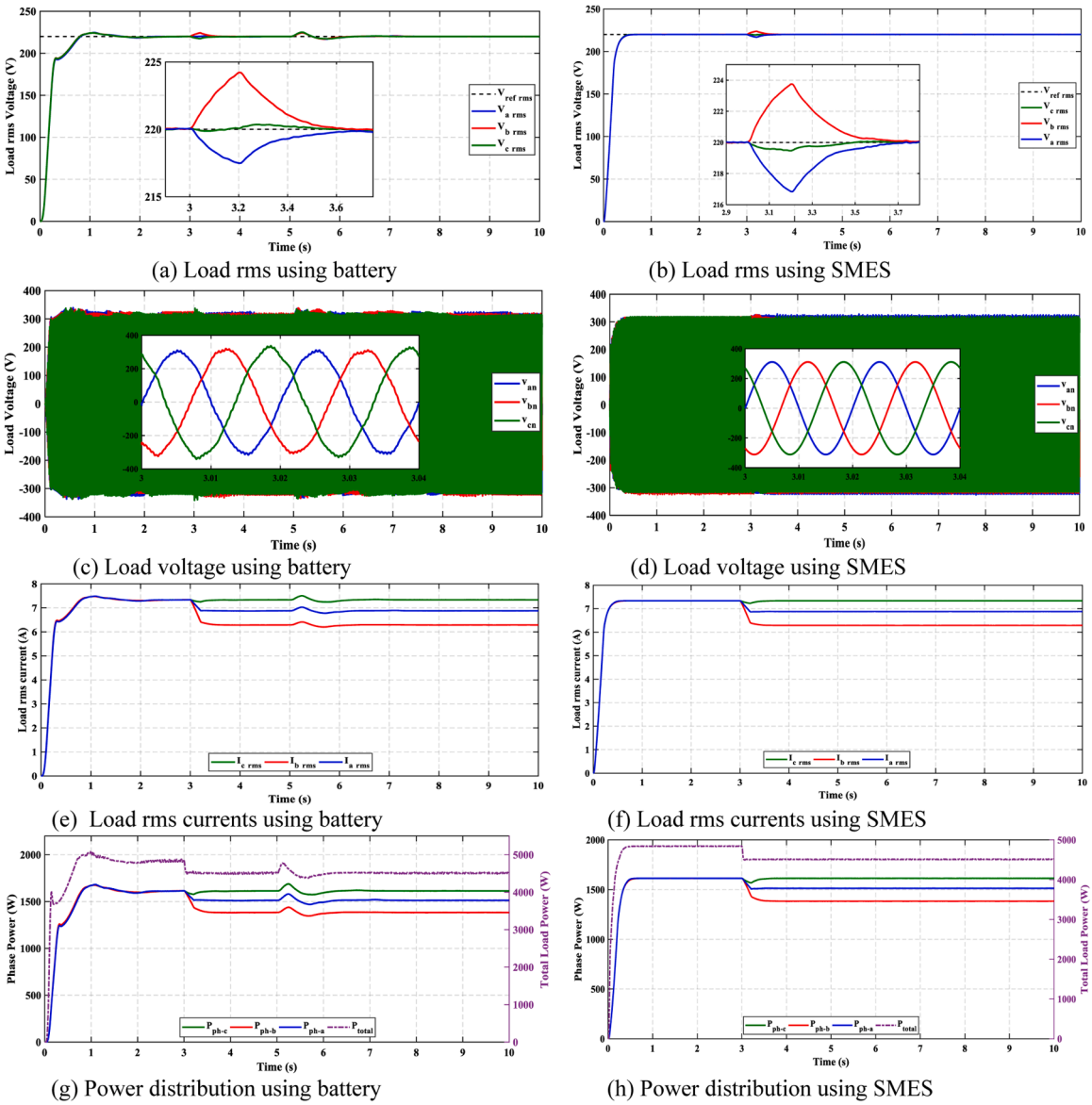

Fig. 31. Results of the unbalanced loading event using the proposed inverter control technique.

storage system by integrating batteries and SMES together in the same energy system. A suitable coordination between the two ESTs can enhance the overall capabilities of the system, reduce the stress on energy storage elements, and prolong their lifetime.

CRediT authorship contribution statement

Kotb M. Kotb: Conceptualization, Methodology, Investigation, Formal analysis, Software, Validation, Data curation, Writing – original

Table 7
Comparison among the proposed study and relative studies.

Ref.PV	MG type	MPPT		Control schemes			Climatic fluctuations	Loading unbalance	Voltage stability
		PV	WT	Battery	SMES	Inverter			
[47]	DC	x	x	PI	x	PI	Slow & Small	No	Yes
[48]	DC	INC	OTC	PI	x	PI	Slow & Small	No	No
[49]	DC	P&O	P&O	FLC	x	PI	Slow & Small	No	No
[50]	AC	INC	x	x	FLC	PI	Normal & Extreme	No	Yes
[51]	AC	INC	x	x	FLC	PI	Slow & Small	No	Yes
[52]	AC	INC	x	x	MPC	MPC	Slow & Small	No	Yes
[53]	DC	SMC	SMC	x	x	x	Fast	No	Yes
[54]	AC	INC	x	x	FLC	PI	Slow & Small	No	No
[55]	DC	INC	x	PI	x	x	x	No	Yes
Proposed	DC	INC	TSR	FLC	FLC	SPWM based-PI	Normal & Extreme	Yes	Yes

Table A1
Overall system parameters and ratings.

Element/Parameter	Value	Element/Parameter	Value
PV module		Wind Turbine	
Maximum power	6.1 kW	Nominal power	7.5 kW
Open circuit voltage	321 V	Cut-in speed	4 m/sec
Short circuit current	18.4 A	Cut-off speed	12 m/sec
Voltage at MPP (V_{MPP})	273.5 V	Blade radius	3.2 m
Current at MPP (I_{MPP})	22.32 A	Inertia	7.5 kg.m2
Parallel strings	4	Friction coefficient	0.06 N.m.s/rad
Series modules/string	5	**SMES**	
The PMSG		Rated capacity	67.5 kJ
Nominal power	6 kW	Coil inductance	1.5 H
Nominal speed	153 rad/sec	Rated current	300 A
Nominal current	12 A	DC-link capacitor	8.6 mF
Nominal torque	40 N.m	**Battery**	
Stator inductance	8.4 mH	Terminal voltage	300 V
Armature resistance	0.4 Ω	Nominal capacity	50 Ahr
		Nominal discharge current	10 A
		Initial SOC	70%

draft, Writing – review & editing. **Mahmoud F. Elmorshedy:** Methodology, Validation, Formal analysis, Writing – review & editing. **Hossam S. Salama:** Investigation, Validation, Formal analysis, Writing – review & editing. **András Dán:** Formal analysis, Software, Writing – review & editing, Supervision.

Declaration of Competing Interest

The authors declare that they have no known competing financial interests or personal relationships that could have appeared to influence the work reported in this paper.

Appendix

Table A1

References

[1] A.N. Abdalla, M.S. Nazir, H. Tao, S. Cao, R. Ji, M. Jiang, et al., Integration of energy storage system and renewable energy sources based on artificial intelligence: an overview, J. Energy Storage 40 (2021), https://doi.org/10.1016/j.est.2021.102811.

[2] A.I. Fahad Saleh, DC microgrid planning, operation, and control: a comprehensive review, IEEE Access 9 (2021) 36154–36172, https://doi.org/10.1109/ACCESS.2021.3062840.

[3] X. Chen, J. Xiao, J. Yuan, Z. Xiao, W. Gang, Application and performance analysis of 100% renewable energy systems serving low-density communities, Renew. Energy 176 (2021), https://doi.org/10.1016/j.renene.2021.05.117.

[4] M.F. Elmorshedy, M.R. Elkadeem, K.M. Kotb, I.B.M. Taha, D. Mazzeo, Optimal design and energy management of an isolated fully renewable energy system integrating batteries and supercapacitors, Energy Convers. Manag. 245 (2021), https://doi.org/10.1016/j.enconman.2021.114584.

[5] IEA (2021), Global Energy Review 2021, IEA, Paris https://www.iea.org/reports/global-energy-review-2021.

[6] S.M. Said, B. Hartmann, Alleviation of extremely power and voltage variations caused by wind power and load demand using SMES, Period Polytech. Electr. Eng. Comput. Sci. 63 (2019), https://doi.org/10.3311/PPee.13718.

[7] K.M. Kotb, M.R. Elkadeem, M.F. Elmorshedy, A. Dán, Coordinated power management and optimized techno-enviro-economic design of an autonomous hybrid renewable microgrid: a case study in Egypt, Energy Convers. Manag. 221 (2020), https://doi.org/10.1016/j.enconman.2020.113185.

[8] D. Mazzeo, N. Matera, P. De Luca, C. Baglivo, P.M. Congedo, G. Oliveti, A literature review and statistical analysis of photovoltaic-wind hybrid renewable system research by considering the most relevant 550 articles: an upgradable matrix literature database, J. Clean. Prod. 295 (2021), https://doi.org/10.1016/j.jclepro.2021.126070.

[9] M. Farhadi, O. Mohammed, Energy storage technologies for high-power applications, IEEE Trans. Ind. Appl. 52 (2016), https://doi.org/10.1109/TIA.2015.2511096.

[10] A.L.A.Z. Shaqsi, K. Sopian, A. Al-Hinai, Review of energy storage services, applications, limitations, and benefits, Energy Rep. 6 (2020), https://doi.org/10.1016/j.egyr.2020.07.028.

[11] A.A. Khodadoost Arani, B.G. Gharehpetian, M. Abedi, Review on energy storage systems control methods in microgrids, Int. J. Electr. Power Energy Syst. 107 (2019), https://doi.org/10.1016/j.ijepes.2018.12.040.

[12] M.S. Guney, Y. Tepe, Classification and assessment of energy storage systems, Renew. Sustain. Energy Rev. 75 (2017), https://doi.org/10.1016/j.rser.2016.11.102.

[13] I. Kouache, M. Sebaa, M. Bey, T. Allaoui, M. Denai, A new approach to demand response in a microgrid based on coordination control between smart meter and distributed superconducting magnetic energy storage unit, J. Energy Storage 32 (2020), https://doi.org/10.1016/j.est.2020.101748.

[14] J.J. Justo, F. Mwasilu, J. Lee, J.W. Jung, AC-microgrids versus DC-microgrids with distributed energy resources: a review, Renew. Sustain. Energy Rev.v 24 (2013), https://doi.org/10.1016/j.rser.2013.03.067.

[15] E. Planas, J. Andreu, J.I. Gárate, I. Martínez de Alegría, E. Ibarra, AC and DC technology in microgrids: a review, Renew. Sustain. Energy Rev. 43 (2015), https://doi.org/10.1016/j.rser.2014.11.067.

[16] M. Faisal, M.A. Hannan, P.J. Ker, A. Hussain, M.M. Bin, F. Blaabjerg, Review of energy storage system technologies in microgrid applications: issues and challenges, IEEE Access 6 (2018), https://doi.org/10.1109/ACCESS.2018.2841407.

[17] M.A.A. Khan, M.M. Shahriar, M.S. Islam, Power Quality improvement of DFIG and PMSG based hybrid wind farm using SMES, in: Proceedings of the 2nd International Conference on Electrical & Electronic Engineering (ICEEE), IEEE, 2017, https://doi.org/10.1109/CEEE.2017.8412899.

[18] H.S. Salama, I. Vokony, Power stability enhancement of SCIG and DFIG based wind turbine using controlled-SMES, Int. J. Renew. Energy Res. 9 (2019) 147–156.

[19] S.M. Said, M. Aly, B. Hartmann, A.G. Alharbi, E.M. Ahmed, SMES-based fuzzy logic approach for enhancing the reliability of microgrids equipped with PV generators, IEEE Access 7 (2019), https://doi.org/10.1109/ACCESS.2019.2927902.

[20] M. Elmorshedy, M.M. Amin, F.F.M. El-Sousy, O.A. Mohammed, DC-bus voltage control of MPPT-based wind generation system using hybrid BESS-SMES system for pulse loads in ship power applications, in: Proceedings of the IEEE Applied Power Electronics Conference and Exposition, IEEE, 2021, https://doi.org/10.1109/APEC42165.2021.9487114.

[21] K.M. Kotb, S.M. Said, A. Dan, B. Hartmann, Stability enhancement of isolated-microgrid applying solar power generation using SMES based FLC, in: Proceedings of the 7th International Istanbul Smart Grids and Cities Congress and Fair, IEEE, 2019, https://doi.org/10.1109/SGCF.2019.8782321.

[22] G. Bharathi, P. Kantharao, R. Srinivasarao, Fuzzy logic control (FLC)-based coordination control of DC microgrid with energy storage system and hybrid distributed generation, Int. J. Ambient Energy (2021), https://doi.org/10.1080/01430750.2021.1874526.

[23] B.R. Al, I. W, T. Mallick, M. Abusara, DC microgrid power coordination based on fuzzy logic control, in: Proceedings of the 18th European Conference on Power

Electronics and Applications (EPE'16 ECCE Europe), IEEE, 2016, https://doi.org/10.1109/EPE.2016.7695530.
[24] J.X. Jin, J. Wang, R.H. Yang, T.L. Zhang, S. Mu, Y.J. Fan, et al., A superconducting magnetic energy storage with dual functions of active filtering and power fluctuation suppression for photovoltaic microgrid, J. Energy Storage 38 (2021), https://doi.org/10.1016/j.est.2021.102508.
[25] A.A.A. Al, B. Y, N. Ullah, H. Abeida, M.S. Soliman, Y.S.H. Khraisat, et al., Hybrid wind/PV/battery Energy management-based intelligent non-integer control for smart dc-microgrid of smart university, IEEE Access 9 (2021), https://doi.org/10.1109/ACCESS.2021.3095973.
[26] A. Kusmantoro, Coordinated control of battery energy storage system based on fuzzy logic for microgrid with modified AC coupling configuration, Int. J. Intell. Eng. Syst. 14 (2021), https://doi.org/10.22266/ijies2021.0430.45.
[27] S.M. Said, H.S. Salama, B. Hartmann, I. Vokony, A robust SMES controller strategy for mitigating power and voltage fluctuations of grid-connected hybrid PV–wind generation systems, Electr. Eng. 101 (2019), https://doi.org/10.1007/s00202-019-00848-z.
[28] M.R. Elkadeem, S. Wang, S.W. Sharshir, E.G. Atia, Feasibility analysis and techno-economic design of grid-isolated hybrid renewable energy system for electrification of agriculture and irrigation area: a case study in Dongola, Sudan, Energy Convers. Manag. 196 (2019) 1453–1478, https://doi.org/10.1016/J.ENCONMAN.2019.06.085.
[29] M.F. Elmorshedy, K.M. Kotb, A. Dan, Hybrid Renewable microgrid system based DC-bus scheme for residential load applications, in: Proceedings of the 22nd International Conference on Electrical Machines and Systems, IEEE, 2019, https://doi.org/10.1109/ICEMS.2019.8922530.
[30] W. Zhang, A. Maleki, M.A. Rosen, A heuristic-based approach for optimizing a small independent solar and wind hybrid power scheme incorporating load forecasting, J. Clean. Prod. 241 (2019), https://doi.org/10.1016/j.jclepro.2019.117920.
[31] U. Eminoglu, O. Turksoy, Power curve modeling for wind turbine systems: a comparison study, Int. J. Ambient Energy (2019), https://doi.org/10.1080/01430750.2019.1630302.
[32] N. Mendis, K.M. Muttaqi, S. Sayeef, S. Perera, Standalone operation of wind turbine-based variable speed generators with maximum power extraction capability, IEEE Trans. Energy Convers. 27 (2012), https://doi.org/10.1109/TEC.2012.2206594.
[33] O. Tremblay, L.A. Dessaint, A.I.A. Dekkiche, Generic battery model for the dynamic simulation of hybrid electric vehicles, in: Proceedings of the IEEE Vehicle Power and Propulsion Conference, IEEE, 2007, https://doi.org/10.1109/VPPC.2007.4544139.
[34] L. Mariam, M. Basu, M.F. Conlon, Microgrid: architecture, policy and future trends, Renew. Sustain. Energy Rev. 64 (2016), https://doi.org/10.1016/j.rser.2016.06.037.
[35] S. Baek, E. Park, M.G. Kim, S.J. Kwon, K.J. Kim, J.Y. Ohm, et al., Optimal renewable power generation systems for Busan metropolitan city in South Korea, Renew. Energy 88 (2016), https://doi.org/10.1016/j.renene.2015.11.058.
[36] H.S. Salama, M.M. Aly, M. Abdel-Akher, I. Vokony, Frequency and voltage control of microgrid with high WECS penetration during wind gusts using superconducting magnetic energy storage, Electr. Eng. 101 (2019), https://doi.org/10.1007/s00202-019-00821-w.
[37] H.S. Salama, I. Vokony, Voltage and frequency control of balanced/unbalanced distribution system using the SMES system in the presence of wind energy, Electricity 2 (2021), https://doi.org/10.3390/electricity2020013.
[38] X. Luo, J. Wang, M. Dooner, J. Clarke, Overview of current development in electrical energy storage technologies and the application potential in power system operation, Appl. Energy 137 (2015), https://doi.org/10.1016/j.apenergy.2014.09.081.
[39] H.S. Salama, I. Vokony, Comparison of different electric vehicle integration approaches in presence of photovoltaic and superconducting magnetic energy storage systems, J. Clean. Prod. 260 (2020), https://doi.org/10.1016/j.jclepro.2020.121099.
[40] S.C. Johnson, F. Todd Davidson, J.D. Rhodes, J.L. Coleman, S.M. Bragg-Sitton, E. J. Dufek, et al., Selecting favorable energy storage technologies for nuclear power. storage hybrid, Nucl. Energy (2019) 119–175, https://doi.org/10.1016/B978-0-12-813975-2.00005-3. Elsevier.
[41] L.A. Zadeh, Fuzzy sets, Inf. Control 8 (1965), https://doi.org/10.1016/S0019-9958(65)90241-X.
[42] F. Liu, S. Duan, F. Liu, B. Liu, Y. Kang, A variable step size INC MPPT method for PV systems, IEEE Trans. Ind. Electron. 55 (2008), https://doi.org/10.1109/TIE.2008.920550.
[43] K.M. Kotb, M.R. Elkadeem, M.F. Elmorshedy, A. Dán, Coordinated power management and optimized techno-enviro-economic design of an autonomous hybrid renewable microgrid: a case study in Egypt, Energy Convers. Manag. 221 (2020), https://doi.org/10.1016/j.enconman.2020.113185.
[44] H. Fathabadi, Maximum mechanical power extraction from wind turbines using novel proposed high accuracy single-sensor-based maximum power point tracking technique, Energy 113 (2016), https://doi.org/10.1016/j.energy.2016.07.081.
[45] L. Barote, C. Marinescu, Modeling and operational testing of an isolated variable speed PMSG wind turbine with battery energy storage, Adv. Electr. Comput. Eng. 12 (2012) 81–88, https://doi.org/10.4316/aece.2012.02014.
[46] K.M. Kotb, M.F. Elmorshedy, A. Dan, Permanence improvement of a local energy production system including unbalanced loading, in: Proceedings of the International IEEE Conference and Workshop in Óbuda on Electrical and Power Engineering, IEEE, 2019, https://doi.org/10.1109/CANDO-EPE47959.2019.9110974.
[47] O. Krishan, S. Suhag, Techno-economic analysis of a hybrid renewable energy system for an energy poor rural community, J. Energy Storage 23 (2019) 305–319, https://doi.org/10.1016/j.est.2019.04.002.
[48] P.S. Sikder, N. Pal, Modeling of an intelligent battery controller for standalone solar-wind hybrid distributed generation system, J. King Saud. Univ. Eng. Sci. 32 (2020) 368–377, https://doi.org/10.1016/j.jksues.2019.02.002.
[49] S. Das, A.K. Akella, Power flow control of PV-wind-battery hybrid renewable energy systems for stand-alone application, Int. J. Renew. Energy Res. 8 (2018) 36–43.
[50] S.M. Said, B. Hartmann, Alleviation of extremely power and voltage variations caused by wind power and load demand using SMES, Period Polytech. Electr. Eng. Comput. Sci. 63 (2019) 134–143, https://doi.org/10.3311/PPee.13718.
[51] H.S. Salama, M.M. Aly, I. Vokony, Voltage/frequency control of isolated unbalanced radial distribution system fed from intermittent wind/PV power using fuzzy logic controlled-SMES, in: Proceedings of the International Conference on Innovative Trends in Computer Engineering, IEEE, 2019, pp. 414–419, https://doi.org/10.1109/ITCE.2019.8646469.
[52] A. Bakeer, H.S. Salama, I. Vokony, Integration of PV system with SMES based on model predictive control for utility grid reliability improvement, Prot. Control Mod. Power Syst. 6 (2021) 14, https://doi.org/10.1186/s41601-021-00191-1.
[53] F. Ez-zahra Lamzouri, E.M. Boufounas, A.E.L. Amrani, Efficient energy management and robust power control of a standalone wind-photovoltaic hybrid system with battery storage, J. Energy Storage 42 (2021), 103044, https://doi.org/10.1016/j.est.2021.103044.
[54] J.X. Jin, J. Wang, R.H. Yang, T.L. Zhang, S. Mu, Y.J. Fan, et al., A superconducting magnetic energy storage with dual functions of active filtering and power fluctuation suppression for photovoltaic microgrid, J. Energy Storage 38 (2021), 102508, https://doi.org/10.1016/j.est.2021.102508.
[55] S. Sinha, P. Bajpai, Power management of hybrid energy storage system in a standalone DC microgrid, J. Energy Storage 30 (2020), 101523, https://doi.org/10.1016/j.est.2020.101523.